Spin transport in half-metallic ferromagnet-superconductor junctions

Chien-Te Wu and Klaus Halterman

Phys. Rev. B **98**, 054518 — Published 30 August 2018

DOI: 10.1103/PhysRevB.98.054518

Spin Transport in Half-Metallic Ferromagnet-Superconductor Junctions

Chien-Te Wu[1,2,*] and Klaus Halterman[3,†]

[1]*Department of Electrophysics, National Chiao Tung University, Hsinchu 30010, Taiwan, Republic of China*
[2]*Physics Division, National Center for Theoretical Sciences, Hsinchu 30010, Taiwan, Republic of China*
[3]*Michelson Lab, Physics Division, Naval Air Warfare Center, China Lake, California 93555*

(Dated: August 10, 2018)

We investigate the charge and spin transport in half-metallic ferromagnet (F) and superconductor (S) nanojunctions. We utilize a self-consistent microscopic method that can accommodate the broad range of energy scales present, and ensures proximity effects that account for the interactions at the interfaces are accurately determined. Two experimentally relevant half-metallic junction types are considered: The first is a F_1F_2S structure, where a half-metallic ferromagnet F_1 adjoins a weaker conventional ferromagnet F_2. The current is injected through the F_1 layer by means of an applied bias voltage. The second configuration involves a $SF_1F_2F_3S$ Josephson junction whereby a phase difference $\Delta\varphi$ between the two superconducting electrodes generates the supercurrent flow. In this case, the central half-metallic F_2 layer is surrounded by two weak ferromagnets F_1 and F_3. By placing a ferromagnet with a weak exchange field adjacent to an S layer, we are able to optimize the conversion process in which opposite-spin triplet pairs are converted into equal-spin triplet pairs that propagate deep into the half-metallic regions in both junction types. For the tunnel junctions, we study the bias-induced local magnetization, spin currents, and spin transfer torques for various orientations of the relative magnetization angle θ in the F layers. We find that the bias-induced equal-spin triplet pairs are maximized in the half-metal for $\theta \approx 90^\circ$ and as part of the conversion process, are anticorrelated with the opposite-spin pairs. We show that the charge current density is maximized, corresponding to the occurrence of a large amplitude of equal-spin triplet pairs, when the exchange interaction of the weak ferromagnet is about $0.1E_F$. For the half-metallic Josephson junctions we often find that the spin current flowing in the half-metal is equivalent to the charge supercurrent flowing throughout the junction. This is indicative that the current consists of spin-polarized triplet pairs. The conversion process of the opposite-spin triplet pairs to the equal-spin triplet pairs in the weaker magnets is clearly demonstrated. This is exemplified by the fact that the supercurrent in the half metal was found to be relatively insensitive to its thickness.

I. INTRODUCTION

Superconductor (S) and ferromagnet (F) hybrids have opened up many new possibilities for further advancements in spintronics devices whose purpose is to manipulate the flow of charge and spin currents[1]. Central to their functionality is experimental control of the spin degree of freedom while enjoying the dissipationless nature of supercurrent. This control is typically afforded through magnetization rotations of one of the free ferromagnetic layers, achieved via weak in-plane external magnetic fields, or by the spin transfer torque (STT) effect. The most commonly studied transport structures based on superconductors and ferromagnets are equilibrium Josephson junctions or voltage biased superconducting tunnel junctions. In any case, the underlying junction architecture often involves spin and charge transport through a spin-valve configuration. A basic superconducting spin-valve consists of two or more ferromagnets adjacent to a superconductor[2–4], where rotation of one of the F layer magnetizations modifies the induced oscillatory singlet pairing in the ferromagnets. If the F layers are half-metallic, these oscillations rapidly dampen out due to their incompatible nature. If however the ferromagnetic regions have non-collinear magnetizations, as will be discussed shortly, triplet pairs with parallel projection of spin can be created that extend deep within the half-metal. In Ref. 5, it is also suggested that magnon excitation plays a role in the conversion between singlet and triplet pairs. These spin-polarized triplet pairs are thus of great interest, and their signatures have been theoretically predicted[6–8] and experimentally observed[9] in the superconducting critical temperature of half-metallic spin valves when rotating one of the F layer magnetizations. Transport measurements in a half-metallic Josephson junction[10,11] demonstrated a supercurrent through the half-metal CrO_2, also indicating the current is carried by equal-spin Cooper pairs since singlet pairs are blocked by the half metal. Because control of the transport of dissipationless spin-currents is a major objective of low-temperature spintronics devices, superconducting junctions that merge half-metallic ferromagnets and superconductors are increasingly being recognized as valuable platforms to study these two competing orders.

Spin currents can flow within superconducting junctions with two or more F layers due to the ferromagnetic exchange interactions. They can also flow with the help of induced equal-spin triplet pairing correlations, where the Cooper pairs have a net spin of $m = \pm 1$ on the spin quantization axis. The generation of these long-range triplet correlations in superconducting heterostructures with magnetic inhomogeneities has been well studied theoretically[12] and experimentally. By introducing magnetic inhomogeneity, e.g., inclusion of multiple magnets with misaligned exchange fields[13], or via the spin-active interface[14,15], the Hamiltonian no longer commutes with the total spin operator and equal-spin triplet correlations can be induced. Due to the imbalance between majority and minority spins in a ferromagnet, conventional singlet pairing correlations decay over short distances within the magnetic region. However, Cooper pairs with electrons that carry the same spin ($m = \pm 1$) are not subject to the paramagnetic pair breaking and can in principle propagate for large

distances inside the ferromagnet, limited only by coherence breaking processes. Such long-range $m = \pm 1$ triplet correlations thus play an important role in Josephson and tunneling junctions containing ferromagnets with noncollinear magnetizations.

While there has been extensive work towards isolating and detecting the triplet pairing state, it can be difficult to disentangle the equal-spin triplet and opposite-spin singlet and triplet correlations. It is therefore of interest to investigate heterostructures that restrict the formation of opposite spin pairs while retaining the desired equal-spin triplet correlations. The pinpointing of triplet effects can be exploited with the use of highly polarized materials like half metallic ferromagnets, where only a single spin channel is present at the Fermi level. The ordinary singlet pairs and opposite-spin triplet pairs are consequently suppressed, as the magnet behaves essentially as an insulator for the opposite spin band. Half-metallic ferromagnets are thus finding increasing use in superconducting spin valves. Several half metallic materials are considered in connection with superconducting hybrids and spintronic applications. These include the manganese perovskite $La_{2/3}Ca_{1/3}MnO_3$[9,16–19], as well as the Heusler compounds such as Cu_2MnAl, which are favorable experimentally, since they can be grown by sputtering techniques[20]. The conducting ferromagnet CrO_2[10,11,21] is also a candidate for use in half-metallic spin valves, although it cannot be grown by sputtering methods, and is metastable.

Experimental signatures of triplet correlations in half-metallic SF_1F_2 spin valves have been demonstrated in transition temperature T_c variations that occur when rotating the magnetization of the free ferromagnet layer[9,21]. Measuring the corresponding maximal change in the critical temperature, ΔT_c, can represent the emergence of spin-polarized triplet pairs as the singlet superconducting state weakens and is subsequently converted into opposite-spin and equal-spin triplet pairs. Most experiments for these types of spin valve structures involved weak ferromagnets for the outer F_2 layer and in-plane magnetic fields, yielding ΔT_c sensitivities from a few mK to around 100 mK[22–26]. When the F_2 layer is replaced by a half-metallic ferromagnet such as CrO_2, a larger ΔT_c of $\Delta T_c \approx 800\,\mathrm{mK}$ was measured[21] using a large out-of-plane applied magnetic field. If $La_{0.6}Ca_{0.4}MnO_3$ is used as the half metallic ferromagnet, a much weaker in-plane magnetic field suffices to rotate the magnetization in one of the F layers[9], resulting $\Delta T_c \approx 150\,\mathrm{mK}$, which again is a stronger spin valve effect compared to experiments involving standard ferromagnets[25,26]. These types of improvements were shown to be consistent with theoretical work[6,7,27] which demonstrated that when the exchange field in F_2 varies from zero to half-metallic, the largest ΔT_c arises when F_2 is a half-metallic. These experimental evidences further established the advantages of utilizing half-metallic elements in superconducting spintronics devices.

Although critical temperature measurements give valuable information regarding half-metallic spin valves, for spintronics devices it is important to also investigate the transport of charge and spin in these types of spin-valve structures. By placing the spin valve between two superconducting banks with a phase difference $\Delta\varphi$, a half-metallic based Josephson junction with spin-controlled supercurrent can be generated. Interest in Josephson junctions with ferromagnetic layers has grown due to their use in cryogenic spintronic systems, including superconducting computers and nonvolatile memories[5,11,14,15,28–37] where their use in single flux quantum circuits can improve switching speeds[38–40]. To determine whether Josephson structures can serve as viable spintronic devices, it is crucial to understand the behavior of the spin currents that can flow in such systems. The interaction between the spin currents and the magnetizations in ferromagnetic Josephson junctions is important for memory applications since the magnetization orientations in the F layers dictates the storage of information bits. Controlling the magnetization rotation can be achieved by a torque from the spin-polarized currents flowing perpendicular to the layers. Some of the spin angular momentum of the polarized current will be transferred to the ferromagnets, giving rise to the STT effect[1,41–45]. This effect can result in a decrease of magnetization switching times in random access memories[46–48]. The STT effect is known to occur in a broad variety of ferromagnetic materials, including half-metals, making it widely accessible experimentally.

In the past, half-metallic Josephson junctions were theoretically studied by using circuit theory[49], recursive Green's function method[33,34], and quasiclassical theory[7,35,50–52]. Results presented in most of the above work concerns the implication of triplet pairs in the current-phase relation due to either magnetic inhomogeneity or interfacial spin-flip scattering. In contrast to previous work, we consider half-metallic Josephson junctions in the clean limit by solving the self-consistent Bogoliubov-de Gennes (BdG) equations, thereby guaranteeing that important conservation laws are obeyed[53]. Such an approach is appropriate because the BdG equations are suitable for the parameter space spanning the nonmagnetic interaction limit to the half-metallic limit. In this paper, we focus on $SF_1F_2F_3S$ Josephson junctions where the central F layer is half metallic. Unlike the relatively uncontrollable spin-flip scattering at the interfaces, the built-in spin valve in $SF_1F_2F_3S$ Josephson junctions offers the advantage of being easily controlled in experiments by applying an external magnetic field.

Since in these half-metallic Josephson junctions the triplet pairs are responsible for the spin supercurrents[10,11], we establish in this work the connection between spin/charge transport and induced triplet correlations to provide insights into the interplay between these important physical quantities. An essential mechanism responsible for supercurrent flow in a half-metallic Josephson junction is Andreev reflection that occurs at the ferromagnet and superconductor interfaces[54–57]. In addition to continuum states, the superposition of localized quasiparticle wavefunctions in the ferromagnet regions results in subgap bound states that contribute to the total current flow. For strong ferromagnets, the corresponding spin-polarized Andreev bound states can be strongly affected by the supercurrent, directly influencing the spin currents and STT when varying the relative in-plane magnetization angle. Although the charge current is conserved, remaining uniform

throughout the sample, the spin current often varies spatially, making comparisons between the two types of current difficult. Moreover, since manipulating the angle between the magnetization vectors can generate long-ranged spin polarized triplet supercurrents[53], these triplet correlations also correlate with spatial variations in the spin currents responsible for the mutual torques acting on the ferromagnets.

As demonstrated in Refs. 58 and 59, these equal-spin triplet pairs result in a more robust Josephson supercurrent that is relatively insensitive to F layer thicknesses due to their long-ranged nature. If one of the ferromagnets in the junction is half-metallic, the equal-spin triplet correlations are expected to play an even greater role in the behavior of the charge and spin currents. This was shown experimentally[10] where a spin triplet supercurrent was measured through the half-metal CrO_2, and whose direction was switchable via magnetization variation. Even in the diffusive limit, it was shown that spin-flip scattering events at the interfaces of a half-metallic Josephson junction also allow penetration of the equal-spin pairs into the half-metal[60]. A triplet current can also be generated when resonantly tuned microwave radiation impinges on a half-metallic Josephson junction, causing a precessing magnetization[5]. Considering the potentially greater control of spin currents afforded by Josephson junctions with strongly spin-polarized ferromagnets, it would be illuminating to systematically investigate the interplay of the triplet pair correlations with the charge and spin transport throughout half-metallic Josephson structures with spin valves separating two superconducting banks.

Another way to produce charge and spin currents in half-metallic spin valve structures involves establishing a voltage difference between the ends of a F_1F_2S tunnel junction, resulting in an injected current into the F_1 layer. The charge and spin transport properties for these types of nonequilibrium tunnel junctions with relatively weak ferromagnets was previously studied[61–63] as functions of bias voltage using a transfer matrix approach that combines the Blonder-Tinkham-Klapwijk (BTK) formalism and self-consistent solutions to the BdG equations. The use of this technique was also extended to accurately compute spin transport quantities, including STT and the spin currents, while ensuring that the appropriate conservation laws are satisfied[61–63]. If the F_1 layer is half-metallic, the current can become strongly polarized, leading to a relatively large transfer of angular momentum to the F_2 layer for noncollinear magnetizations, via the STT effect. Also, the angularly averaged subgap conductance in this case arises mainly from anomalous Andreev reflection[19,61,64], whereby a reflected hole with the same spin as the incident particle is Andreev reflected, generating a spin-polarized triplet pair.

The BTK approach applied to either tunneling structures or Josephson junctions with the presence of half metals have been adopted in the past[36,37,64,65]. The scattering approach is also a useful scheme to study the conductance of tunneling junctions when a half metal is present[66–68]. The effects of applied bias on spin-polarized tunneling conductance and STT has also been previously studied in superconducting tunnel junctions[69] in the small bias regime. By applying an external magnetic field, or through switching via STT, it is again possible to control the relative orientation of the intrinsic magnetizations and investigate the dependence of the charge and spin currents on the misorientation angle θ between the two ferromagnetic layers. Thus, when a half-metallic layer is present in a F_1F_2S tunnel junction, we can have greater control and isolation of the spin currents and spin-polarized triplet pairs that are critical for viable spintronics platforms. The systematic investigation into the transport and corresponding triplet correlations of half-metallic spin valves for nonequilibrium tunnel junctions is another main focus of this work. By extending the formalism adopted in Ref. 61, we have successfully computed the bias dependence of the induced equal-spin triplet pair amplitudes and identify their relationship with the charge transport.

When considering spin transport in superconducting junctions, it is beneficial for the structure to contain both weakly polarized and strongly polarized ferromagnets. This is because the singlet and the opposite spin triplet correlations in weaker ferromagnets extend over greater lengths, dictated by the inverse of the exchange field, making them much more effective at hosting opposite-spin pairs. The weak ferromagnet serves as an intermediate layer between the superconductor and half-metal, facilitating the generation of opposite-spin pairs that will eventually become converted into the longer ranged equal-spin triplet pairs. A hybrid ferromagnetic setup also creates an avenue for the systematic investigation into the interplay and ultimate control of both triplet channels. We therefore are interested in two types of superconducting junctions with spin-valve structures in this paper. The first consists of a single superconductor in contact with two ferromagnets (the F_1F_2S structure), with the inner F_2 ferromagnet having a weak exchange field, and the outer F_1 being half-metallic. The current in this nonequilibrium case is injected by means of a voltage difference between two electrodes.

As alluded to earlier, the other scenario involves a Josephson junction containing a half-metal flanked by two weaker conventional ferromagnets. The current is established in the usual way by a macroscopic phase difference $\Delta\varphi$ between the two outer superconducting banks. For both junction arrangements, we investigate the charge and spin transport within the ballistic regime using a microscopic self-consistent BdG formalism that is capable of accommodating the broad range of energy scales set by the exchange field h of the conventional ferromagnets ($h/E_F \ll 1$) and the half-metal ($h = E_F$). Of crucial importance towards the theoretical description of these type of transport structures is to accurately be able to account for the mutual interactions between the ferromagnetic and superconducting elements, i.e., proximity effects. This requires a self-consistent treatment, which ensures that the final solutions minimize the free energy of the system and satisfies the proper conservation laws. This numerical approach is a time-consuming but necessary step to reveal the self-content proximity effects that govern the nontrivial charge and spin currents that flow within these structures. Indeed, the tunneling conductance in F_1F_2S junctions was shown to differ substantially from that obtained via a non-self-consistent approach[61]. Therefore, our microscopic, self-consistent treatments enable

us to especially focus on the connections between spin and charge transport and the long-ranged nature of superconductivity.

This paper is organized as follows: In Sec. II A, we present the general Hamiltonian and self-consistent BdG methodology that is applicable for both junction configurations. In Sec. II B, the transfer matrix approach for tunnel junctions that combines the Blonder-Tinkham-Klapwijk (BTK) formalism and self-consistent solutions to the BdG equations is established. The charge continuity equation and current density are also derived. In Sec. II C, the relevant details for the characterization of equilibrium half-metallic Josephson junctions and the expression for the associated current density are given. In Sec. II D, we outline how to calculate the induced triplet correlations for equilibrium Josephson junctions and non-equilibrium tunnel junctions. In Sec. II E the techniques used to compute the spin transport quantities including magnetization, spin-transfer torque, and the spin current are derived for both types of junctions. Throughout Sec. II, we discuss how to properly satisfy the conservation laws for charge and spin densities in our formalism. In Sec. III A we present the results for half-metallic tunnel junctions. Results for the spatial dependence to the bias-induced magnetizations, the spin-transfer torque, the spin currents, and triplet correlations are presented as functions of the magnetization misalignment angle as well as the applied bias. We also report how to take advantage of the induced triplet correlations by choosing the optimal exchange interactions in F layers. In Sec. III B, we present the results for the half-metallic Josephson junctions, including the current phase relations for a variety of half-metal thicknesses. The spatial dependencies to the spin currents and triplet correlations are given, and a broad range of misalignment angles are considered to demonstrate the propagation of spin-polarized triplet pairs through the half-metal. The positive correlations between the equal-spin triplet correlations and the spin-polarized supercurrents are also discussed. We conclude with a summary in Sec. IV.

II. METHODS

A. Description of the systems

Two types of half-metallic junctions are considered in this paper: tunneling junctions and Josephson junctions. The effective Hamiltonian that is applicable to both types of junctions is

$$\begin{aligned}\mathcal{H}_{\text{eff}} = \int d^3r \Bigg\{ & \sum_s \psi_s^\dagger(\boldsymbol{r}) H_0 \psi_s(\boldsymbol{r}) \\ & + \frac{1}{2}\left[\sum_{s\,s'} \left(i\sigma_y\right)_{ss'} \Delta(\boldsymbol{r}) \psi_s^\dagger(\boldsymbol{r}) \psi_{s'}^\dagger(\boldsymbol{r}) + H.c.\right] \\ & - \sum_{s\,s'} \psi_s^\dagger(\boldsymbol{r}) \left(\boldsymbol{h}\cdot\boldsymbol{\sigma}\right)_{ss'} \psi_{s'}(\boldsymbol{r})\Bigg\}, \end{aligned} \tag{1}$$

where H_0 is the single-particle part of $\mathcal{H}_{\text{eff}}$, $\boldsymbol{h}$ describes exchange interaction of the magnetism, s and s' are spin indices and $\boldsymbol{\sigma}$ are Pauli matrices. $\Delta(\boldsymbol{r}) \equiv g(\boldsymbol{r})\langle\psi_\uparrow(\boldsymbol{r})\psi_\downarrow(\boldsymbol{r})\rangle$ is the superconducting pair potential and $g(\boldsymbol{r})$ is the coupling constant. In ferromagnets where there is no intrinsic superconducting pairing, $g(\boldsymbol{r})$ is taken to be zero. Similarly, $\boldsymbol{h}$ vanishes in intrinsically superconducting regions. Following Ref. 61, we utilize the generalized Bogoliubov transformation[70], $\psi_s = \sum_n \left(u_{ns}\gamma_n + \eta_s v_{ns}^*\gamma_n^\dagger\right)$, where $\eta_s \equiv 1(-1)$ for spin-down (up), to write down the BdG Hamiltonian equivalent to Eq. (1):

$$\begin{aligned}&\begin{pmatrix} H_0 - h_z & -h_x + ih_y & 0 & \Delta \\ -h_x - ih_y & H_0 + h_z & \Delta & 0 \\ 0 & \Delta^* & -(H_0 - h_z) & -h_x - ih_y \\ \Delta^* & 0 & -h_x + ih_y & -(H_0 + h_z) \end{pmatrix}\begin{pmatrix} u_{n\uparrow} \\ u_{n\downarrow} \\ v_{n\uparrow} \\ v_{n\downarrow} \end{pmatrix} \\ &= \epsilon_n \begin{pmatrix} u_{n\uparrow} \\ u_{n\downarrow} \\ v_{n\uparrow} \\ v_{n\downarrow} \end{pmatrix}, \end{aligned} \tag{2}$$

where u_{ns} and v_{ns} in the generalized Bogoliubov transformations can be identified as the quasiparticle and quasihole amplitudes, respectively.

For layered tunnel junctions and Josephson junctions considered in this work, we assume each F and S layer is infinite in the yz plane and the layer thicknesses extend along the x axis (See Figs. 1 and 7). As a result, the BdG Hamiltonian [Eq. (2)] is translationally invariant in the yz plane, and it becomes quasi-one-dimensional in x. The single-particle Hamiltonian is $H_0 = -(1/2m)(d^2/dx^2) + \epsilon_\perp - E_F$, where we have defined the transverse kinetic energy as $\epsilon_\perp \equiv (k_y^2 + k_z^2)/2m$, and E_F denotes the Fermi energy. Although in this work, we do not consider Fermi energy mismatch between distinct layers, it is straightforward to include such an effect. Throughout this paper, we take $\hbar = k_B = 1$, and all energies are measured in units of E_F. We numerically determine the pair potential by using fully self-consistent solutions to Eq. (2). The iterative self-consistent procedure has been extensively discussed in previous work[61,71]. Since our BdG Hamiltonian is quasi-one-dimensional, the pair potential is only a function of x. By minimizing the free energy of the system, and making use of the generalized Bogoliubov transformation, the pair potential can be written as,

$$\Delta(x) = \frac{g(x)}{2}{\sum_n}' \left[u_{n\uparrow}(x)v_{n\downarrow}^*(x) + u_{n\downarrow}(x)v_{n\uparrow}^*(x)\right]\tanh\left(\frac{\epsilon_n}{2T}\right), \tag{3}$$

where T is temperature and the prime symbol means that a Debye cutoff energy, ω_D, is introduced in the energy sum. Additional details of our formalism used in this work can also be found in Refs. 53 and 61.

B. Tunnel junctions

We begin first with tunnel junctions depicted in Fig. 1 where a ferromagnet and half metal are in contact with a superconductor. The ferromagnet that is not adjacent to S is labeled F_1, and the one next to S is F_2. As shown in Fig. 1, the exchange field in F_1 is $h_1\hat{\boldsymbol{z}}$, and in F_2 it is $h_2(\sin\theta\hat{\boldsymbol{y}} + \cos\theta\hat{\boldsymbol{z}})$.

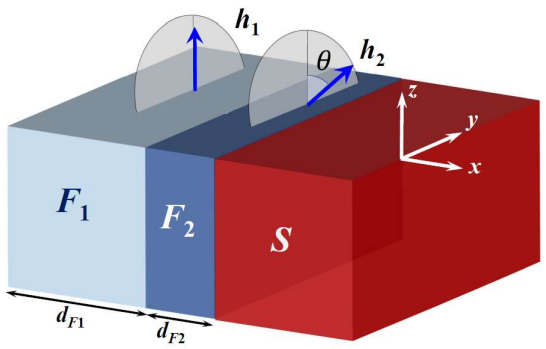

FIG. 1. (Color online) Illustration of the F_1F_2S tunnel junction that is infinite and translationally invariant in the yz plane. It has finite size along the x axis. F_1 is a half-metal and the associated exchange field is fixed along the z direction. The direction of the exchange field in F_2 is in the yz plane, and makes an angle θ with the z axis. Such a misorientation can be achieved experimentally via an external magnetic field.

Here h_1 and h_2 are the magnitudes of the exchange fields in F_1 and F_2, respectively. In general, we consider F_1 as a fixed layer where the exchange field is pinned and F_2 as a free layer where the relative angle θ can be controlled by an applied magnetic field experimentally[23]. In this work, we take the fixed layer F_1 to be a half metal and $h_1 = E_F$.

In previous work[61], a formalism based on the BTK approach[72] was generalized to study spin-transport quantities. In Ref. 72, it was shown, starting from the Boltzmann equation, that the conductance associated with the tunnel junction is a function of the transmission and reflection amplitudes in the linear response regime. Therefore, to compute the tunneling conductance, one should start by writing down the appropriate wavefunctions in each distinct region. The details of this procedure is given in the Appendix. Following this procedure, the formula for the spin-dependent conductance, normalized to that of the normal state in the low temperature regime, is given by

$$G_s = 1 + \frac{k^-_{\uparrow 1}}{k^+_{s1}}\left|a_{s\uparrow}\right|^2 + \frac{k^-_{\downarrow 1}}{k^+_{s1}}\left|a_{s\downarrow}\right|^2 - \frac{k^+_{\uparrow 1}}{k^+_{s1}}\left|b_{s\uparrow}\right|^2 - \frac{k^+_{\downarrow 1}}{k^+_{s1}}\left|b_{s\downarrow}\right|^2, \quad (4)$$

where $\left|a_{s\uparrow}\right|^2$ and $\left|a_{s\downarrow}\right|^2$ are the amplitudes of the Andreev reflected waves, and $\left|b_{s\uparrow}\right|^2$ and $\left|b_{s\downarrow}\right|^2$ are the amplitudes of the normally reflected waves. In the above expression, the subscript s denotes the spin type of the incident wave into the F_1 region. For example, $a_{\uparrow\downarrow}$ corresponds to the process whereby a spin-down hole is reflected when a spin-up particle is incident. Here, the k's represent the corresponding wavevectors, with the $+(-)$ superscript dictating the particle (hole) nature of the reflected wave, and the subscript 1 denoting the F_1 region. For example, $k^-_{\uparrow 1}$ is the wavevector of a spin-up hole wavefunction in F_1.

In Ref. 61, the BTK formalism has been generalized to study transport quantities such as spin currents and spin transfer torques. By applying the transfer matrix method outlined in the Appendix A, these position dependent quantities can be properly computed. For a non-zero bias, V, across the electrodes of a F_1F_2S junction, a non-equilibrium quasi-particle distribution is generated. In the excitation picture, it is clear that all states with energies $\epsilon < eV$ incident from the electrode in F_1 to the electrode in S should be taken into account in the low T limit[61]. Hence, the respective charge density and current density are given by:

$$\rho = -e\sum_{ns}|v_{ns}|^2 - e\sum_{\epsilon_k<eV}\sum_s\left(|u_{\boldsymbol{k}s}|^2 - |v_{\boldsymbol{k}s}|^2\right), \quad (5)$$

$$J_x = -\frac{e}{m}\mathrm{Im}\left[\sum_{\epsilon_k<eV}\sum_s\left(u^*_{\boldsymbol{k}s}\frac{\partial u_{\boldsymbol{k}s}}{\partial x} + v^*_{\boldsymbol{k}s}\frac{\partial v_{\boldsymbol{k}s}}{\partial x}\right)\right], \quad (6)$$

where we sum over states labeled by their momenta $\boldsymbol{k}$ with energies less than the bias voltage. It is easy to see from the above equations that when $V = 0$, $J_x = 0$, and ρ is just the ground-state charge density, as one would expect. In nonequilibrium situations, the conservation law for charge flow [see Eq. (B2) in the Appendix] contains a source term, which in the presence of the bias, becomes: $-4e\mathrm{Im}\left[\Delta\sum_{\epsilon_k<eV}\left(u^*_{k\uparrow}v_{k\downarrow} + v_{k\uparrow}u^*_{k\downarrow}\right)\right]$. We emphasize here that Δ vanishes in the intrinsically non-superconducting region since the coupling constant is taken to be zero there. Hence, on the F side the divergence (spatial derivative) of the current vanishes and the current is a constant. On the S side, where Δ exists, the derivative of the current does not vanish. This does not mean that the conservation law for charge current is violated, as the right-hand-side describes the process of interchange between the quasi-particle current density and the supercurrent density, as clearly discussed in Ref. 61 and 72.

C. Josephson junctions

We next discuss the pertinent aspects of the half-metallic Josephson junctions that we shall investigate. As shown in Fig. 7, we consider $S_1F_1F_2F_3S_2$ type junctions, where the central half-metallic layer F_2 is surrounded by two ferromagnets F_1 and F_3. We will show below in Sec. III B that it is important for the ferromagnets to be thin (relative to ξ_F, the superconducting proximity length) and for them to have relatively weak exchange fields so that their placement near the superconducting banks allows for the generation of triplet correlations and the associated phase coherent transport. The exchange fields in each of the junction layers reside in-plane and are written

$$\boldsymbol{h}_i = h_i(\sin\theta_i\hat{\boldsymbol{y}} + \cos\theta_i\hat{\boldsymbol{z}}), \quad \text{for } i = 1, 2, 3. \quad (7)$$

To compute the dc Josephson current where the bias across the junction is absent, we again numerically look for solutions by iteratively solving Eq. (2), which is very general and can be applied to both the F_1F_2S tunneling and $S_1F_1F_2S_2$ Josephson junctions. Since we wish to determine the current-phase relation for the Josephson junctions, the initial input for the pairing potential is taken to be the bulk gap, Δ_0, in

S_1 and $\Delta_0 \exp(i\Delta\varphi)$ in S_2. With this input, Eq. (2) is then numerically diagonalized and the new pair potential, $\Delta(x)$ is computed from Eq. (3) throughout the entire junction except for small regions (around one coherence length, ξ_0, from the sample edges) considered as boundaries of the junctions. In these regions, the pair potential is fixed to its bulk absolute value, with phases 0 and $\Delta\varphi$, respectively. The newly yielded $\Delta(x)$ is then used in the BdG equations and the above process is repeated iteratively until convergence is achieved. When current is flowing through the junction, the self-consistently calculated regions are always found to possess the necessary spatially constant current. The important distinction between tunneling and Josephson junctions is the presence of the external bias. For dc Josephson junctions, the bias is absent and the source term of the continuity equation should always vanish in order to not violate the conservation law. One can also write down the charge supercurrent associated with a fixed nonzero phase difference between S_1 and S_2. The expression for the current density in a Josephson junction is given by

$$J_x = -\frac{e}{m}\sum_{ns}\mathrm{Im}\left[u_{ns}\frac{\partial u^*_{ns}}{\partial x}f_n + v_{ns}\frac{\partial v^*_{ns}}{\partial x}(1-f_n)\right], \tag{8}$$

where f_n is the Fermi function. If the phase of the order parameter is a constant throughout the junction, the current density vanishes as can be seen from Eq. (8). We emphasize here that Eq. (8) is applicable only when the external bias is absent. Nevertheless, both Eqs. (6) and (8) are derived using the Heisenberg approach.

D. Triplet correlations

As discussed in the introduction, for half-metallic superconducting junctions, the induced spin-triplet Cooper pairs play an important role in both equilibrium and transport properties. These triplet pairing correlations are defined as

$$f_0(\boldsymbol{r},t) = \frac{1}{2}\left[\langle\psi_\uparrow(\boldsymbol{r},t)\psi_\downarrow(\boldsymbol{r},0)\rangle + \langle\psi_\downarrow(\boldsymbol{r},t)\psi_\uparrow(\boldsymbol{r},0)\rangle\right], \tag{9a}$$

$$f_1(\boldsymbol{r},t) = \frac{1}{2}\left[\langle\psi_\uparrow(\boldsymbol{r},t)\psi_\uparrow(\boldsymbol{r},0)\rangle - \langle\psi_\downarrow(\boldsymbol{r},t)\psi_\downarrow(\boldsymbol{r},0)\rangle\right], \tag{9b}$$

$$f_2(\boldsymbol{r},t) = \frac{1}{2}\left[\langle\psi_\uparrow(\boldsymbol{r},t)\psi_\uparrow(\boldsymbol{r},0)\rangle + \langle\psi_\downarrow(\boldsymbol{r},t)\psi_\downarrow(\boldsymbol{r},0)\rangle\right], \tag{9c}$$

where the subscript 0 corresponds to $m_s = 0$, and the subscripts 1 and 2 refer to the $m_s = \pm 1$ projections on the spin quantization axis. It was shown in previous work that using this approach to find both the opposite-spin and equal-spin triplet pairs, satisfies the Pauli exclusion principle, and that the triplet pairs vanish at $t = 0$[73,74]. If the exchange fields between in F layers are not collinear, or equivalently, $\theta_i \neq 0$, the total spin operator of the pairs does not commute with the effective Hamiltonian [Eq. (1)], and the long-ranged, spin-polarized components f_1 and f_2 can be induced[73,74]. By using the generalized Bogoliubov transformation and the Heisenberg equations of motion, it is possible to write the field operators in Eqs. (9) as,

$$f_0(x,t) = \frac{1}{2}\sum_n\left[u_{n\uparrow}(x)v^*_{n\downarrow}(x) - u_{n\downarrow}(x)v^*_{n\uparrow}(x)\right]\zeta_n(t), \tag{10a}$$

$$f_1(x,t) = -\frac{1}{2}\sum_n\left[u_{n\uparrow}(x)v^*_{n\uparrow}(x) + u_{n\downarrow}(x)v^*_{n\downarrow}(x)\right]\zeta_n(t), \tag{10b}$$

$$f_2(x,t) = -\frac{1}{2}\sum_n\left[u_{n\uparrow}(x)v^*_{n\uparrow}(x) - u_{n\downarrow}(x)v^*_{n\downarrow}(x)\right]\zeta_n(t), \tag{10c}$$

where $\zeta_n(t) \equiv \cos(\epsilon_n t) - i\sin(\epsilon_n t)\tanh(\epsilon_n/2T)$ and we have assumed zero bias for the junctions. The triplet amplitudes in Eqs. (10a)-(10c) pertain to a fixed quantization axis along the z-direction. In situations where it is more convenient to align the spin quantization axis with the local magnetization direction, we rotate it using the transformations in the Appendix. The exchange field orientations in each layer are described by the angle θ_i, and thus we write,

$$f_0' = \cos\theta_i f_0 + i\sin\theta_i f_2, \tag{11a}$$

$$f_1' = f_1, \tag{11b}$$

$$f_2' = \cos\theta_i f_2 + i\sin\theta_i f_0, \tag{11c}$$

where the prime denotes the rotated system.

The triplet correlations given in Eqs. (10) are only applicable to both static and dynamic equilibrium situations when the external bias is absent. When $V \neq 0$ and in the limit $T \to 0$, Eqs. (9) are bias dependent and we have the following contributions in addition to Eqs. (10),

$$\delta f_0(x,t) = 2i\sum_{\epsilon_k<eV}\left(u_{k\uparrow}(x)v^*_{k\downarrow}(x) - u_{k\downarrow}(x)v^*_{k\uparrow}(x)\right)\sin(\epsilon_k t), \tag{12a}$$

$$\delta f_1(x,t) = 2i\sum_{\epsilon_k<eV}\left(u_{k\uparrow}(x)v^*_{k\uparrow}(x) + u_{k\downarrow}(x)v^*_{k\downarrow}(x)\right)\sin(\epsilon_k t), \tag{12b}$$

$$\delta f_2(x,t) = 2i\sum_{\epsilon_k<eV}\left(u_{k\uparrow}(x)v^*_{k\uparrow}(x) - u_{k\downarrow}(x)v^*_{k\downarrow}(x)\right)\sin(\epsilon_k t). \tag{12c}$$

Apparently, the bias-dependence of Eqs. (9) is entirely given by Eqs. (12).

E. Spin transport

We now discuss the appropriate expressions for spin transport quantities. We expect that with either an external bias or a macroscopic phase difference $\Delta\varphi$ between two S banks, there will be a leakage of magnetism due to a spin-transfer torque[53,61]. The local magnetization is related to the spin density and defined as,

$$\boldsymbol{m}(\boldsymbol{r}) = -\mu_B\langle\boldsymbol{\eta}(\boldsymbol{r})\rangle \equiv -\mu_B\sum_{ss'}\langle\psi^\dagger_s(\boldsymbol{r})\boldsymbol{\sigma}_{ss'}\psi_{s'}(\boldsymbol{r})\rangle, \tag{13}$$

where $\boldsymbol{\eta}(\boldsymbol{r})$ is the spin density operator and μ_B the Bohr magneton. Again, by using the generalized Bogoliubov transformation, each component of $\boldsymbol{m}$ can be written in terms of the

quasiparticle and quasihole wavefunctions:

$$m_x = -2\mu_B \sum_n \mathrm{Re}\left[u_{n\uparrow}u^*_{n\downarrow}f_n - v_{n\uparrow}v^*_{n\downarrow}(1-f_n)\right] \tag{14a}$$

$$m_y = 2\mu_B \sum_n \mathrm{Im}\left[u_{n\uparrow}u^*_{n\downarrow}f_n + v_{n\uparrow}v^*_{n\downarrow}(1-f_n)\right] \tag{14b}$$

$$m_z = -\mu_B \sum_n \left[\left(|u_{n\uparrow}|^2 - |u_{n\downarrow}|^2\right)f_n + \left(|v_{n\uparrow}|^2 - |v_{n\downarrow}|^2\right)(1-f_n)\right], \tag{14c}$$

where we have suppressed the x dependence.

The expression for the spin current density can be again derived from the Heisenberg equation (see Appendix B). It is reduced from a tensor to a vector due to the quasi-one-dimensional nature of our geometry. Therefore, the three components of the spin current vector are associated with those of spin densities and spin current flowing along the x direction, which is perpendicular to the interfaces. These three components can also be expressed in terms of the quasiparticle and quasihole amplitudes:

$$S_x = \frac{\mu_B}{2m}\sum_n \mathrm{Im}\left[\left(u^*_{n\uparrow}\frac{\partial u_{n\downarrow}}{\partial x} + u^*_{n\downarrow}\frac{\partial u_{n\uparrow}}{\partial x}\right)f_n - \left(v_{n\uparrow}\frac{\partial v^*_{n\downarrow}}{\partial x} + v_{n\downarrow}\frac{\partial v^*_{n\uparrow}}{\partial x}\right)(1-f_n)\right], \tag{15a}$$

$$S_y = -\frac{\mu_B}{2m}\sum_n \mathrm{Re}\left[\left(u^*_{n\uparrow}\frac{\partial u_{n\downarrow}}{\partial x} - u^*_{n\downarrow}\frac{\partial u_{n\uparrow}}{\partial x}\right)f_n - \left(v_{n\uparrow}\frac{\partial v^*_{n\downarrow}}{\partial x} - v_{n\downarrow}\frac{\partial v^*_{n\uparrow}}{\partial x}\right)(1-f_n)\right], \tag{15b}$$

$$S_z = \frac{\mu_B}{2m}\sum_n \mathrm{Im}\left[\left(u^*_{n\uparrow}\frac{\partial u_{n\uparrow}}{\partial x} - u^*_{n\downarrow}\frac{\partial u_{n\downarrow}}{\partial x}\right)f_n + \left(v_{n\uparrow}\frac{\partial v^*_{n\uparrow}}{\partial x} - v_{n\downarrow}\frac{\partial v^*_{n\downarrow}}{\partial x}\right)(1-f_n)\right]. \tag{15c}$$

When the junctions are in static equilibrium, the spin-current does not necessarily vanish because any inhomogeneous magnetization leads to a non-zero spin-transfer torque thereby causing a net spin current[53,61]. The spin current $\boldsymbol{S}$ is a local physical quantity, and $\boldsymbol{\tau}$ is responsible for the change in local magnetizations due to the flow of spin-polarized currents [see Eq. (B5) in the Appendix]. As we shall see in Sec. III, this conservation law (with the source torque term) for the spin density is a fundamental relation, and one has to ensure that it is not violated when studying these transport quantities.

The above expressions, Eqs. (14) and Eqs. (15), are applicable only when the external bias is zero. Let us go back and discuss the bias dependence of spin transport quantities for F_1F_2S tunneling junctions. As in the discussion on the triplet correlations, we first define the bias induced magnetization as $\delta\boldsymbol{m}(V) \equiv \boldsymbol{m}(V) - \boldsymbol{m}_0$, where $\boldsymbol{m}_0$ is given by Eqs. (14) and $\boldsymbol{m}(V)$ is the total magnetization with the presence of a finite bias. In the low-T limit, the bias induced magnetization reads,

$$\delta m_x = -\mu_B \sum_{\epsilon_k<eV}\left(u^*_{k\uparrow}u_{k\downarrow} + v_{k\uparrow}v^*_{k\downarrow} + u^*_{k\downarrow}u_{k\uparrow} + v_{k\downarrow}v^*_{k\uparrow}\right), \tag{16a}$$

$$\delta m_y = -i\mu_B \sum_{\epsilon_k<eV}\left(u^*_{k\uparrow}u_{k\downarrow} + v_{k\uparrow}v^*_{k\downarrow} - u^*_{k\downarrow}u_{k\uparrow} - v_{k\downarrow}v^*_{k\uparrow}\right), \tag{16b}$$

$$\delta m_z = -\mu_B \sum_{\epsilon_k<eV}\left(|u_{k\uparrow}|^2 - |v_{k\uparrow}|^2 - |u_{k\downarrow}|^2 + |v_{k\downarrow}|^2\right). \tag{16c}$$

Similarly, we can define the corresponding bias induced spin currents, $\delta\boldsymbol{S}(V) \equiv \boldsymbol{S}(V) - \boldsymbol{S}_0$, where $\boldsymbol{S}_0$ is identitcal to Eqs. (15). The bias induced spin currents are given by

$$\delta S_x = -\frac{\mu_B}{m}\mathrm{Im}\left[\sum_{\epsilon_k<eV}\left(u^*_{k\uparrow}\frac{\partial u_{k\downarrow}}{\partial y} + v_{k\uparrow}\frac{\partial v^*_{k\downarrow}}{\partial y} + u^*_{k\downarrow}\frac{\partial u_{k\uparrow}}{\partial y} + v_{k\downarrow}\frac{\partial v^*_{k\uparrow}}{\partial y}\right)\right], \tag{17a}$$

$$\delta S_y = \frac{\mu_B}{m}\mathrm{Re}\left[\sum_{\epsilon_k<eV}\left(u^*_{k\uparrow}\frac{\partial u_{k\downarrow}}{\partial y} + v_{k\uparrow}\frac{\partial v^*_{k\downarrow}}{\partial y} - u^*_{k\downarrow}\frac{\partial u_{k\uparrow}}{\partial y} - v_{k\downarrow}\frac{\partial v^*_{k\uparrow}}{\partial y}\right)\right], \tag{17b}$$

$$\delta S_z = -\frac{\mu_B}{m}\mathrm{Im}\left[\sum_{\epsilon_k<eV}\left(u^*_{k\uparrow}\frac{\partial u_{k\uparrow}}{\partial y} - v_{k\uparrow}\frac{\partial v^*_{k\uparrow}}{\partial y} - u^*_{k\downarrow}\frac{\partial u_{k\downarrow}}{\partial y} + v_{k\downarrow}\frac{\partial v^*_{k\downarrow}}{\partial y}\right)\right]. \tag{17c}$$

In short, the finite bias leads to a nonequilibrium quasiparticle distribution for the system, and results in non-static spin current densities that are represented by Eqs. (17). Finally, we note that the spin-transfer torque has to vanish in the superconductor where the exchange field is zero.

III. RESULTS

A. Tunneling Junctions

We begin this section by first discussing our numerical results on F_1F_2S tunneling junctions as illustrated in Fig. 1. The thicknesses of F_1, F_2, and S layers are taken to be $300/k_F$, $10/k_F$, and $130/k_F$, respectively. These thicknesses are fixed throughout this subsection. The superconducting coherence length is also fixed to be $100/k_F$. We consider clean interfaces between these layers. In other words, interfacial scattering events are not taken into account in this subsection (the main consequence from these events would be to reduce the proximity effects). For our half-metallic tunneling junctions, the exchange fields in F_1, the layer that is farthest from the superconductor, is $h_1 = E_F$ (see Fig. 1). All energy scales are measured with respect to the Fermi energy. As will be demonstrated below, the spin-valve effect is maximized when the exchange field of the ferromagnet F_2 is relatively weaker, approximately on the order of $h_2 = 10^{-1}E_F$.

Most of the previous theoretical work based on either BTK approach or scattering matrix formalism focuses on the tunneling conductance of half-metallic superconducting spin valves[61,64–66]. It is found that the tunneling conductance in

the subgap region is governed by the same-spin Andreev reflection. As a result, the subgap conductance vanishes at zero-bias and grows linearly in the subgap region. Since results on the tunneling conductance of half-metallic superconducting spin valves have been extensively studied in the literature, we therefore are mainly interested in spin transport quantities including magnetization, spin current, and spin transfer torque. As clearly explained in Ref. 61, even in the static limit where the bias across the junction is absent, the spin current and the spin transfer torque in general do not vanish near the interface between two F layers as long as the magnetic configuration is noncollinear. Since dynamical transport properties are the main concern in the current work, and in order to clearly see the bias dependence of these spin-dependent quantities, for most of our results in this subsection we will restrict ourselves to the dynamic part that is induced by the external bias. For example, the "induced" magnetizations, $\delta\boldsymbol{m}(V)$ are defined in Eqs. (16). We conveniently normalize the magnetization by $-\mu_B n_e$, where $n_e = k_F^3/3\pi^2$ is the electron number density. Similarly, the induced spin currents, $\delta\boldsymbol{S}(V)$, and the induced STT, $\delta\boldsymbol{\tau} \equiv \boldsymbol{\tau}(V) - \boldsymbol{\tau}(V=0)$, are normalized by $-\mu_B n_e E_F/k_F$, and by $-\mu_B n_e E_F$, respectively. Below we shall discuss the position dependence of all spin transport quantities. For convenience, we measure lengths in units of k_F^{-1} and use $X \equiv k_F x$ to denote positions.

In Fig. 2, we present the angular dependence of the induced magnetizations, spin currents, and spin-transfer torques for the half-metallic spin valve shown in Fig. 1. The half-metallic layer F_1 is adjacent to a thinner and relatively weak ferromagnet with $h_2 = 10^{-1}E_F$. We begin by giving simple physical reasons for choosing these parameters. The thickness of F_2 is chosen to be thin compared to F_1 and S in order to take advantage of the superconducting proximity effects. For the same reason, the exchange field in F_2 also needs to be weak enough to study the interplay between the superconducting proximity effects and spin-valve effects. In our coordinate system, $X = 0$ corresponds to the interface between F_2 and S. Therefore, in Fig. 2, the half-metal F_1 lies in the range $X < -10$, the superconductor is in the region $X > 0$, and the F_2 layer is in the region $-10 < X < 0$. The bias across the junction is set to be $2\Delta_0$ in the figure, where Δ_0 is the singlet pair amplitude in the bulk limit. Recall that in our considerations, the exchange field in F_1 is along the $\hat{z}$ axis and in F_2 it is tilted with respect to the $\hat{z}$ axis by an angle θ in the yz plane. There are two main effects that need to be taken into account in order to understand the induced magnetizations: First, the magnetic moments in F_1 and F_2 interact, with the magnetization of F_1 leaking into F_2, and vice versa, resulting in spatial precession. Secondly, both the direction and magnitude of the static magnetic moments in F_2 will affect any induced magnetizations when an external bias is present.

For the three components of the induced magnetizations (Panels (a)-(c) in Fig. 2), we first see that δm_x and δm_y vanish throughout the entire junction when $\theta = 0^\circ$ and 180°. This is because the contributions from both the precession and static magnetizations are zero when the exchange fields are parallel ($\theta = 0^\circ$) or anti-parallel ($\theta = 180^\circ$) to each other. Let us first focus on δm_x for other relative angles. The magnitudes for θ and $\pi - \theta$ are of the same order in the S region because the x component of the static magnetization is not present (recall that the exchange fields in our system are always in-plane, i.e. the yz plane) and only the precession effect is at work. Turning to the δm_y panel, its magnitude in S for $\theta = 90^\circ$ (the exchange field in F_2 is along y) is determined purely from the static magnetization because the precession effect will only affect δm_x and δm_z at this angle. Physically, this tells us that the system becomes spin-polarized in the xy plane in S. When $90^\circ < \theta < 180^\circ$, the contribution to δm_y from the precession effect is negative while the contribution from the effect of the static magnetization in F_2 is positive. The cumulative result is that the magnitudes are much smaller than their counterparts for $0^\circ < \theta < 90^\circ$ in the S region. For δm_z, we can see that it is the only non-zero component throughout the junction for parallel ($\theta = 0^\circ$) and anti-parallel ($\theta = 180^\circ$) configurations. The behaviors for other relative angles are simply explained again by the precession effect, just as in the case for δm_x.

Next, we analyze the behaviors of the induced spin currents and spin transfer torques. The spin-transfer torques are determined by the local exchange fields and magnetization vectors [see Eq. (B7) in the Appendix], which are in turn related to the spin currents given in Eqs. (15) and (17). This is clearly seen in the steady state, where their interplay is encapsulated by the expression, $\frac{\partial \boldsymbol{S}}{\partial y} = \tau$. More generally, one can intuitively understand the role of the induced spin currents $\delta\boldsymbol{S}$ by considering the static magnetizations in each of the ferromagnetic layers. The F_1 layer is relatively thick, and can be regarded as a spin source, which polarizes the incoming current along the $+z$ direction. When a spin current originating from F_1 flows into F_2, the polarization state can be rotated by means of the local exchange field in F_2 and corresponding induced STT. For the z component of the induced spin currents, δS_z, at $\theta = 0^\circ$, it is constant throughout the entire junction including the superconducting layer as the spin density along z commutes with the Hamiltonian. The same argument holds for the other collinear orientation $\theta = 180^\circ$. However, the magnitude of δS_z is larger at $\theta = 0^\circ$ than at $\theta = 180^\circ$, as a consequence of the exchange fields in the F_1 and F_2 layers being oppositely directed while $h_1 \gg h_2$. In fact, the magnitude of δS_z is higher when $\theta < 90^\circ$ than the counterparts at $\pi - \theta$, for exactly the same reasons. Although δS_z at $\theta = 90^\circ$ vanishes inside the superconductor, we found that in general, this is not necessarily the case. The magnitude and the sign of δS_z depend on both the thickness of F_2 and the strength of the exchange field. Thus, by carefully choosing the thickness of the second ferromagnet, which plays an important role in both triplet proximity effects and spin-transfer torques, in principle the spin transport properties of spintronics devices can be manipulated experimentally.

Let us now turn our attention to the remaining components, δS_x and δS_y. In the collinear configurations ($\theta = 0^\circ$ and $\theta = 180^\circ$), both the x and y components are zero because of the absence of the precession effect. Both the sign and magnitude of δS_y in the S region roughly follow the y component of the exchange field in F_2. Although the y component of the exchange field in F_2 is at its maximum when $\theta = 90^\circ$, we find that the corresponding δS_y in S is smaller than when at the

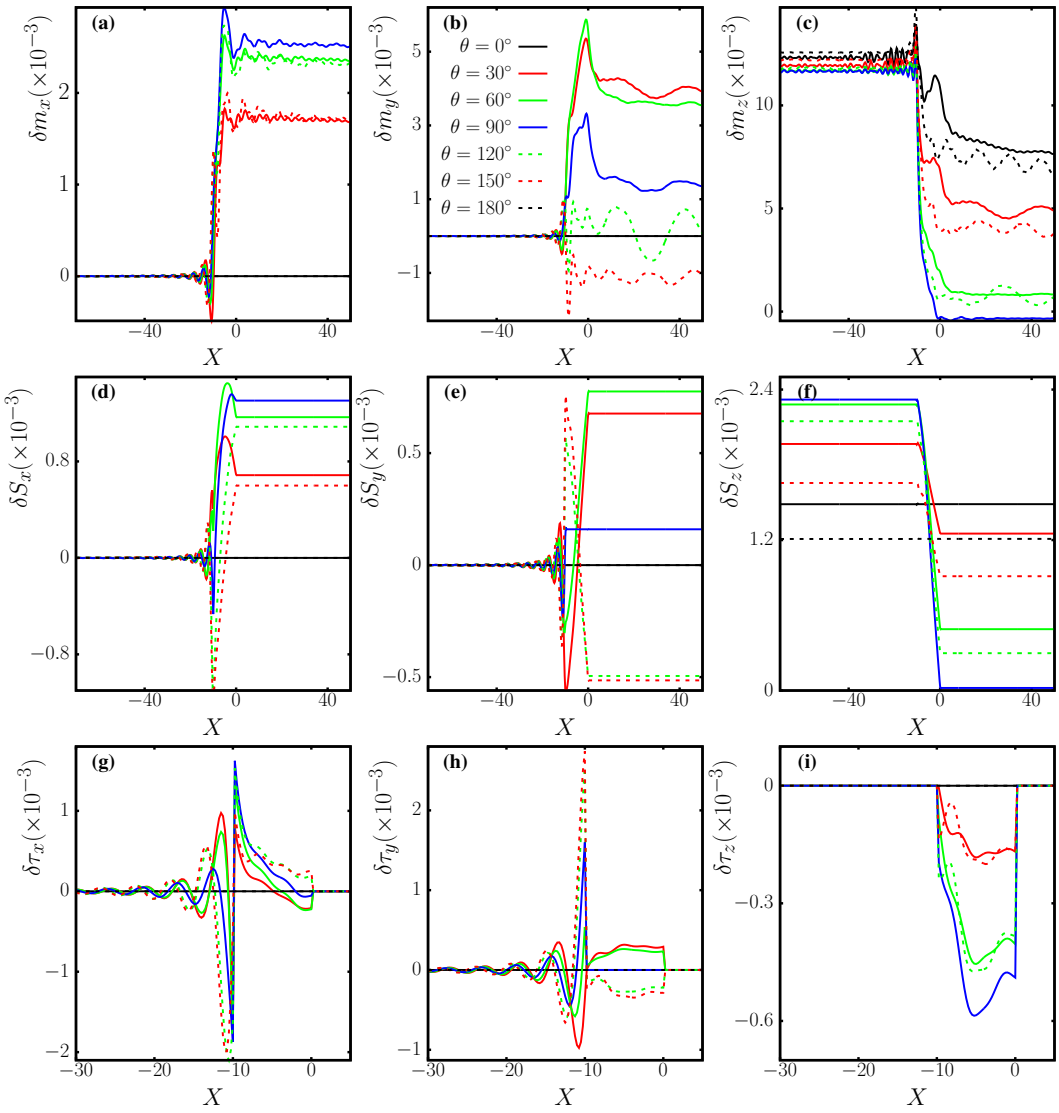

FIG. 2. (Color online) In this figure, we present spin transport quantities as functions of position, $k_F x \equiv X$, for several relative angles, θ, between the exchange fields in the F_1 and F_2 layers of half-metallic F_1F_2S tunneling junctions. The external bias is set to be twice of the bulk superconducting pair amplitude, $V = 2\Delta_0$. The thicknesses of F_1, F_2, and S are set to be $300/k_F$, $10/k_F$, and $130/k_F$, respectively. Panels (a)-(c) in the first row show the dynamical part, $\delta\boldsymbol{m}$, of the three magnetization components, computed from Eqs. (16). Panels (d)-(f) in the second row depicts each component of the dynamical part of the spin currents, $\delta\boldsymbol{S}$, according to Eqs. (17). Spin currents are in general third-rank tensors in three-dimensional space. However, since our system is quasi-one-dimensional, they are reduced to three-dimensional vectors. Panels (g)-(i) in the third row presents the dynamical part of the three components of the spin-transfer torque $\delta\boldsymbol{\tau}$, by using the relation $\delta\boldsymbol{\tau} = \delta\boldsymbol{m} \times \boldsymbol{h}$. From the figure, one can easily verify the formula $\delta\tau_i = \partial S_i/\partial x$ for all θ.

other angles. This is because when $\theta \neq 90°$, the y component of the spin density can still be induced via the spin density precession coming from the half-metallic layer that possesses a much larger magnetization strength, which in turn is more dominant than the other effect. For the same reason, δS_y in S is higher at θ than at $\pi - \theta$, where $\theta < 90°$. The precession effect is seen to play an important role as well in the behavior of δS_x, where as panel (d) shows, at $\theta = 90°$, the dynamical part δS_x abruptly increases in F_2, and then uniformly extends into the S region where it is maximized.

The last interesting quantity is the spin-transfer torque, which is numerically determined using the relations involving the self-consistently calculated $\delta\boldsymbol{m}$ and the exchange field $\boldsymbol{h}$ [see Eq. (B7) in the Appendix]. Since $\boldsymbol{h}$ vanishes identically inside the superconductor, all components of $\delta\boldsymbol{\tau}$ must vanish there. The absence of a torque in the superconductor imposes that the spin current there cannot vary in space [see Eq. (B5) in the Appendix]. Thus the constancy of the spin currents inside the superconducting region shown in Fig. 2. It is also straightforward to understand why $\delta\tau_z = 0$ in the half-metal F_1. We find that $\delta\tau_z$ is maximized in F_2 when $\theta = 90°$, suggesting that the corresponding δS_z must have the greatest change in F_2. Indeed, as can be seen in panel (f), the only spatially varying region is in the ferromagnet F_2, and it occurs the greatest

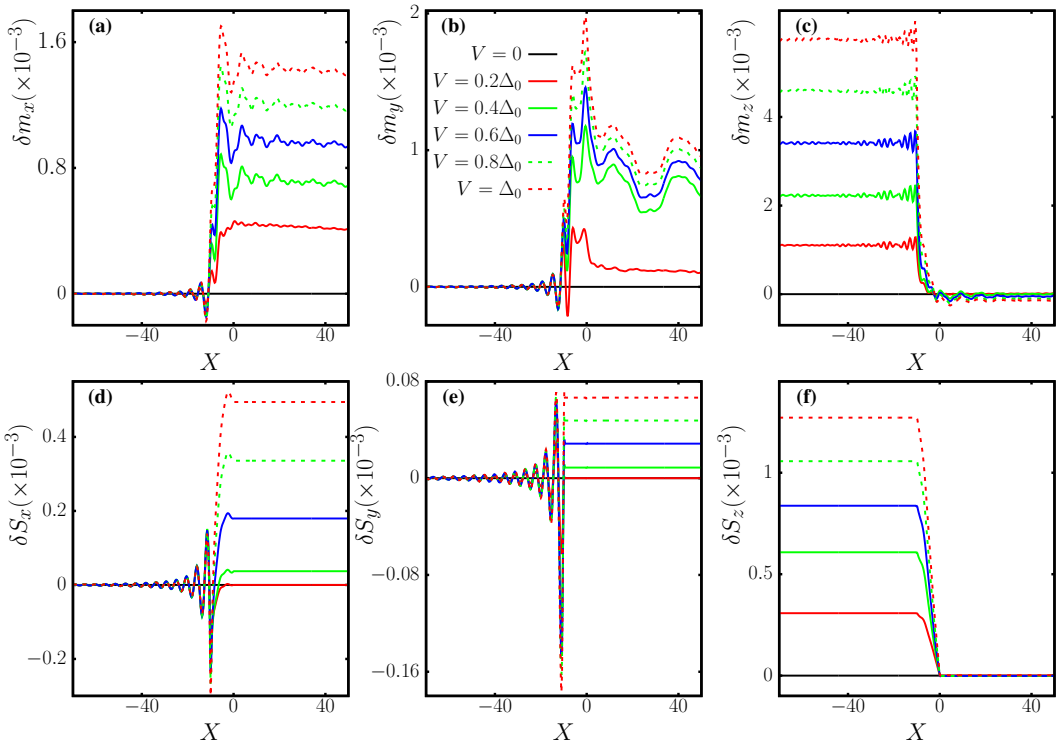

FIG. 3. (Color online) In this figure, we present spin transport quantities as functions of position, $k_F x \equiv X$, for several external biases, V, scaled by the bulk superconducting gap, Δ_0, in half-metallic F_1F_2S tunneling junctions. The relative angle θ between exchange fields in F_1 and F_2 is set to be 90°. The thicknesses of F_1, F_2, and S are set to be $300/k_F$, $10/k_F$, and $130/k_F$, respectively. Panels (a)-(c) in the first row show the dynamical part, $\delta\boldsymbol{m}(V)$, of the three magnetization components, computed from Eqs. (16). Panels (d)-(f) in the second row show the dynamical part, $\delta\boldsymbol{S}(V)$, of the three spin current components, computed from Eqs. (17).

when $\theta = 90°$. We emphasize here that the static part of τ_x is in general non-vanishing as long as the in-plane exchange fields are non-collinear in the F_1F_2S tunneling junctions. The static part of τ_x is much larger than the dynamic part. Therefore, the behavior S_x does not significantly change with the presence of bias (not shown). In panel (e), it was observed that the precessional effect combined with the magnetization rotation in F_2, led to a reversal in the bias-induced spin current variation as θ changed. These abrupt changes in δS_x translate into torque reversals within the relatively weaker ferromagnet region, as well as drastic variations near the F_1/F_2 interface, as demonstrated in (h).

In the linear-response regime, transport quantities are in principle dependent on the external bias, V. However, with the presence of superconductors, transport quantities sometimes exhibit distinct behavior above and below the superconducting gap. The related transport phenomena including excess current and tunneling conductance are thoroughly discussed in Refs. 61 and 72. This gap-dependent feature can be attributed to Andreev reflections. When the external bias is below the superconducting gap, current is not suppressed due to the mechanism of the Andreev scattering. Once the external bias is above the gap, the contribution to current from ordinary scattering emerges. As explained in Sec. II, the superconducting pair amplitudes are determined self-consistently and the gap profiles are position-dependent, which saturate deep inside the bulk superconductor. The saturation values of the gap profiles are important and usually smaller than the bulk superconducting gap, Δ_0. Furthermore, the saturation values also depend on the relative magnetization angle, θ.

In Fig. 3, we plot spin transport quantities at several different biases for $\theta = 90°$. The thicknesses of each layer and exchange interactions are the same as in Fig. 2. Our self-consistent calculations reveal that the saturation value for the superconducting gap is approximately $0.3\Delta_0$. First, we note the trivial fact that the dynamic part of all spin transport quantities vanishes when $V = 0$. We then pay particular attention to the behavior above and below the saturation point $0.3\Delta_0$. Note that all three components of $\delta\boldsymbol{m}$ do not significantly change qualitatively with increased bias, and the major quantitative change is their magnitudes. Nevertheless, $\delta m_y(V = 0.2\Delta_0)$ is greatly suppressed compared to $\delta m_y(V > 0.2\Delta_0)$ while $\delta m_x(V = 0.2\Delta_0)$ is not. We also see that the magnitudes of both δm_x and δm_y increase linearly with V for $V > 0.3\Delta_0$. On the other hand, δm_z does not show very distinct behavior above or below $0.3\Delta_0$, and it increases linearly in the entire V range we considered here.

For the dynamic part of the spin currents $\delta\boldsymbol{S}$, we find that δS_x and δS_y disappear inside the superconducting region when $V < 0.3\Delta_0$. This is due to the fact that any spin polarized current entering the superconductor is converted into a supercurrent, which is spin unpolarized. For $V > 0.3\Delta_0$, the

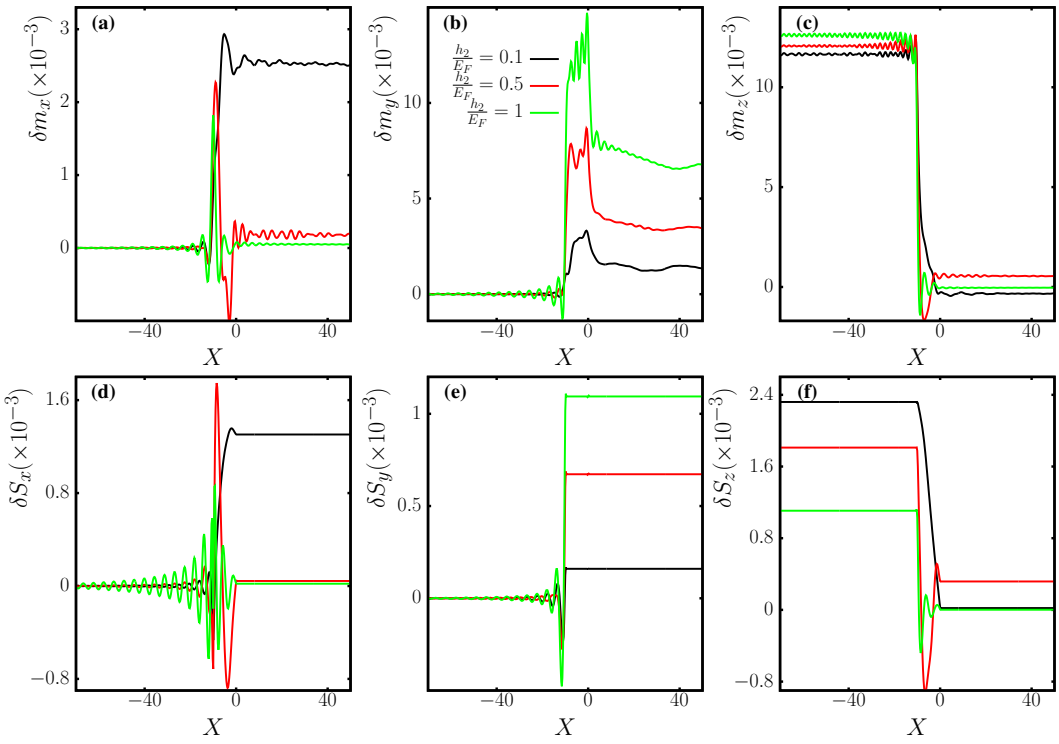

FIG. 4. (Color online) In this figure, we present spin transport quantities as functions of position, $k_F x \equiv X$, for three different h_2 measured in terms of the Fermi energy for half-metallic F_1F_2S tunneling junctions. The external bias is fixed to be twice the bulk superconducting gap, $V = 2\Delta_0$. The relative angle θ between exchange fields in F_1 and F_2 is also fixed and its value is 90°. The thicknesses of F_1, F_2, and S are set to be $300/k_F$, $10/k_F$, and $130/k_F$, respectively. Panels (a)-(c) in the first row show the dynamical part, $\delta\boldsymbol{m}(V = 2\Delta_0)$, of the three magnetization components, computed from Eqs. (16). Panels (d)-(f) in the second row show the dynamical part, $\delta\boldsymbol{S}(V = 2\Delta_0)$, of the three spin current components, computed from Eqs. (17).

magnitudes inside the superconductor increase linearly with the bias, similar to what was found for δm_x and δm_y. At these larger bias voltages, δS_x and δS_y within the half-metal are insensitive to changes in V. Examining panel (f), the current entering the F_1 region becomes strongly polarized by the half-metal, and δS_z increases nearly linearly with greater bias before decaying away after interacting with the adjacent ferromagnet whose exchange field is orthogonal to it (along y). It is evident that unlike δS_x, there are no abrupt changes in behavior about the saturation point $0.3\Delta_0$. Examining the top row of Fig. 3, one can infer the qualitative behavior of the torque throughout the structure. Thus, the bias dependence to the spin transfer torque is omitted here, as it clearly follows that of $\delta\boldsymbol{m}$.

Next, we explore spin transport properties with different strengths of the exchange field in F_2 while fixing the exchange field in F_1 to be $h_1 = E_F$. In Fig. 4, we plot $\delta\boldsymbol{m}$ (top row) and $\delta\boldsymbol{S}$ (bottom row) for three different h_2. The relative angle between the exchange fields in F_1 and F_2 is again fixed at $\theta = 90°$ (the direction of the exchange interaction in F_2 is along y), and the bias is set at $V = 2\Delta_0$. In panel (b), we see that the overall trends in the induced magnetization do not change significantly for different h_2, where δm_y is damped out in the half-metal, and then peaks in F_2 before propagating into the superconductor. The half-metal has its exchange field aligned in the z direction, thus the current is initially polarized in this direction leading to a nearly vanishing y component of the induced magnetization, which becomes y polarized when entering adjacent ferromagnet. The result is that δm_y from both F_1 (due to the precession effect) and F_2 (due to the inherent magnetization) extend into the superconductor with a magnitude proportional to h_2. For the induced magnetization normal to the interfaces, δm_x, we see that it builds up within F_2, and then undergoes damped oscillations (see panel (a)). The period of these oscillations in F_2 are governed by the degree of spin polarization in the ferromagnet and thus scale inversely proportional to h_2. Therefore, one can see that for such a thin F_2, δm_x with $h_2 = 0.1$ is too confined to possess even a full period of oscillation. As a result, when $h_2 = 0.1E_F$, δm_x becomes "squeezed" and has a larger magnitude in F_2 compared to when $h_2 = 0.5E_F$ and $h_2 = E_F$. If we increase the thickness of F_2, δm_x for $h_2 = 0.1E_F$ will also become negligible inside the S layer. This property provides a way for experimentalists to control the flow of magnetization by varying the thickness of the intermediate ferromagnetic layer. Turning now to panel (c), it is seen that inside F_1, δm_z is only very weakly dependent on h_2 and is uniform in space. Inside F_2 it exhibits damped oscillations, akin to δm_x, with an oscillation period that is inversely proportional to h_2. If the F_2 layer is thick enough, δm_z will vanish identically inside the S layer, irrespective of h_2. This sensitivity to thickness can be used to control not only whether δm_z vanishes in the S layer,

but also for appropriate thicknesses, whether it can be positive or negative.

Now, let us compare spin currents for different h_2. From panel (e), we see that for a given h_2, the induced δS_y is constant and flows uninterrupted inside both the F_2 and S layers. This is a reflection of the fact that the y component of the spin-transfer torque vanishes in those regions. This can also be found by simply computing the cross product between $\delta\boldsymbol{m}$ and $\boldsymbol{h}$. For the same reasons, δS_x is constant inside the S layers only, while δS_z is constant in the F_1 and S regions. For each h_2, the relative magnitudes of $\delta\boldsymbol{S}$ in F_2 and the superconducting region follow similar trends as $\delta\boldsymbol{m}$, in that there is a positive correlation between the corresponding components of $\delta\boldsymbol{S}$ and $\delta\boldsymbol{m}$. We also find that the spatial period for the oscillation inside the F_2 layer is the same as that of $\delta\boldsymbol{m}$ for a given h_2. Finally, it is important to stress that both the direction and the magnitude of $\delta\boldsymbol{S}$ can also be adjusted by changing the F_2 thickness. In practice, one would like to choose a weaker ferromagnet for this intermediate layer. This follows not only from the potential triplet pair enhancement (discussed below), but also when a strong ferromagnet is adopted, the F_2 thickness should be relatively thin in order to take advantage of this thickness sensitivity. As before, we do not present the spin-transfer torques here since they can be computed directly from knowledge of $\delta\boldsymbol{m}$ [Fig. 4, first row], and $\boldsymbol{h}$.

We now focus on the induced triplet correlations for these half-metallic tunneling F_1F_2S junctions. It is useful to recall that the triplet correlations can be induced even in the absence of an external bias[71]. As discussed in Ref. 71, triplet correlations with $m = \pm 1$ projections on the spin quantization axis are important since these spin-polarized pairs are immune to pair-breaking effects of the exchange fields in the F layers. This is especially relevant when a very strong half-metallic layer is present. Successful control of a dissipationless supercurrent is regarded as one of the essential goals in the development of practical low-temperature spintronics devices. Presumably, this can be achieved by generating and controlling the f_1 and f_2 equal-spin triplet pairs[53], since they are able to propagate over relatively long distances without serious degradation. To simplify the discussions below, we shall focus on the f_1 equal-spin and f_0 opposite-spin triplet channels, since in many cases f_2 behaves complimentary to f_1.

The physics of induced triplet correlations for spin valves in the static limit has been extensively discussed in Ref. 71. Also, we find that in the F_1 layer the dynamic part is added constructively to the static part of the triplet amplitudes. Therefore, we focus here on the dynamical situation where the external bias is non-vanishing and confine our attention to the dynamic part of the induced triplet correlations. To find the bias dependence to the triplet pairs in our system, we define, similar to previous quantities, the induced triplet correlations via $\delta f_i(V) = f_i(V) - f_i(V = 0)$, where $i = 0, 1$.

In Fig. 5, we present the angular dependence of both the opposite-spin f_0 and equal-spin f_1 triplet pairs. The pair correlations are functions of their relative time difference t, which is set according to the dimensionless relation $\omega_D t = 4.0$. The external bias is fixed at $V = 2.0\Delta_0$. The thicknesses are the same as in previous figures, with the exchange fields in F_1 and F_2 again corresponding to $h_1/E_F = 1$ and $h_2/E_F = 0.1$, respectively. For δf_0 shown in the top panel (a), we find that it decays into the half-metallic layer with a very short decay length, as it is energetically unstable due to the presence of a single spin band at the Fermi level. Within the thin ferromagnet ($-10 < X < 0$), δf_0 is largest when a single quantization axis can be ascribed to the system, i.e., when the magnetizations of both F layers are collinear. There is a slightly more pronounced effect when θ corresponds to the antiparallel configuration, where there are greater competing effects between the magnetizations in the F_1 and F_2 layers. When F_1 and F_2 are in the orthogonal configuration with $\theta = 90°$, they are then in their most inhomogenous magnetic state, and the δf_0 amplitude is lowest in F_2. For other orientations that are closest to the orthogonal configurations, such as $\theta = 60°$, δf_0 is also relatively weak compared to the collinear situation, but larger compared to $\theta = 90°$ due a finite z component to the magnetization. These findings for the thin ferromagnet layer carry over to the superconducting layer, where the following angular dependence is observed: δf_0 is minimized at $\theta = 90°$ (orthogonal configuration) and maximized for the collinear configurations ($\theta = 0°$ and $180°$).

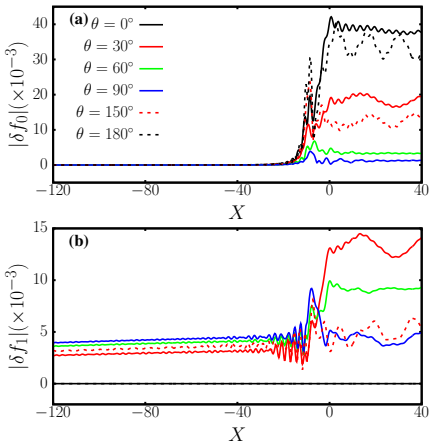

FIG. 5. (Color online) The dynamical part of the induced triplet correlations as functions of position, X, for several angles θ. In panel (a) we have $\delta f_0(V = 2\Delta_0)$ [see Eq. (12a)], and in panel (b) we have $\delta f_1(V = 2\Delta_0)$ [see Eq. (12b)]. The external bias is fixed to be twice that of the bulk superconducting gap, $V = 2\Delta_0$. The relative time of these triplet correlation is $\omega_D t = 4$. The thicknesses of F_1, F_2, and S are set to be $300/k_F$, $10/k_F$, and $130/k_F$, respectively. The exchange fields are $h_1 = E_F$ and $h_2 = 0.1E_F$.

We turn now to the more interesting δf_1 component, which is much more robust against the magnetic pair-breaking effects. In the bottom panel (b), we present the spatial behavior of δf_1, again for several θ. We first see that δf_1 vanishes for the collinear configuration, as it should, as explained earlier in the introduction. For other relative angles, δf_1 is generated because of the non-collinear magnetic profile which prevents the system from being described by a single quantization axis. Furthermore, as shown in panel (b), the bias-induced δf_1 triplet amplitude is long-ranged in the half-metal and maximized for orientations around $\theta = 90°$. This is the central result of this subsection. Once the spin-polarized triplet pairs

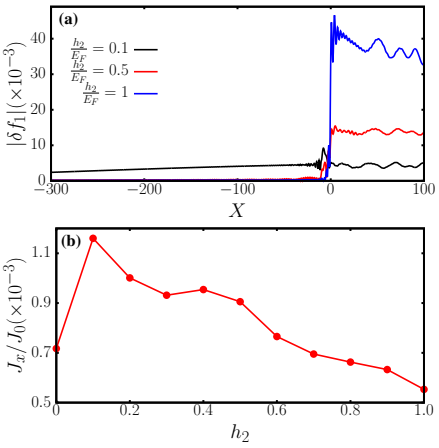

FIG. 6. (Color online) In panel (a) of this figure, we present the dynamical part of induced triplet correlations, δf_1, as functions of position, X, for three different normalized exchange fields in the F_2 layer: $h_2/E_F = 0.1$, $h_2/E_F = 0.5$, and $h_2/E_F = 1.0$. The angle θ between exchange fields in F_1 and F_2 is chosen to be $\theta = 90°$. The external bias is fixed at twice the bulk gap, $V = 2\Delta_0$. The thicknesses of F_1, F_2, and S are set at $300/k_F$, $10/k_F$, and $130/k_F$, respectively. In panel (b), we show the normalized charge current density v.s. the exchange field h_2 of the intermediate F layer. The data points are connected by lines to serve as guides to the eye. The relative angle between the exchange fields in F_1 and F_2 is 90°.

pass through F_2, they enter the superconductor and become enhanced, not for the orthogonal configuration, but rather for slight misalignments in the relative magnetizations. These trends are similar to what was observed in Fig. 2 for the y-component of the bias induced magnetization. Thus, we have demonstrated the long-range nature of the dynamic part of the triplet pairs by showing that only the δf_1 component survives in the half-metal. Also, due to the interactions between F layers and triplet conversion effects, spin-polarized triplets were shown to be effectively generated within the S region. Moreover, our study revealed that δf_0 in F_2 and S, and δf_1 in the half-metal are often anticorrelated, i.e.,when δf_0 is maximized (minimized), δf_1 is minimized (maximized).

It was mentioned at the beginning of this subsection that our choice of $h_2/E_F = 0.1$ for the exchange field strength in the thin intermediate F_2 layer, resulted in the optimal amount of spin-polarized pairs in the half-metallic region. To illustrate this, it is insightful to consider differing exchange field magnitudes in F_2 and examine how these differences affect the equal-spin triplet pairs throughout the entire junction. Thus, we present in panel (a) of Fig. 6, the spatial dependence of the magnitude of the dynamic part δf_1 for several h_2. We set $\theta = 90°$, creating the most magnetically inhomogenous configuration possible, and thus maximizing δf_1 in F_1. Note that here the spatial range is much wider than the results presented before in order to identify any long range behavior of the spin-polarized triplet correlations. First, inside the superconducting layer, we find that the magnitude of δf_1 is approximately proportional to h_2. However, in the non-superconducting regions, δf_1 for both $h_2/E_F = 0.5$ and $h_2/E_F = 1.0$ decays with a very small characteristic decay length. On the other hand, the weaker exchange field of $h_2/E_F = 0.1$ results in δf_1 penetrating quite extensively into the F regions, thereby establishing its long range behavior. This result is significant, and it justifies our choice of for h_2, mentioned earlier. Although we do not show the static part of the induced triplet correlations, we find the same behavior as before: the static part of f_1 is long-ranged when the magnetic configuration is non-collinear and its magnitude is comparable to the dynamic part. In the absence of a bias voltage, the corresponding static f_1 amplitudes are also maximized when $h_2 \sim 0.1E_F$.

To further corroborate these ideas, we show in panel (b) of Fig. 6 the charge current density, J_x, along the direction perpendicular to the interface as a function of h_2. The current density is normalized by $J_0 \equiv en_e v_F$, where $v_F \equiv k_F/m$ is the Fermi velocity. Here we fix the external bias to be $V = 2.0\Delta_0$ and the relative angle between the exchange fields in the F_1 and F_2 layers is $\theta = 90°$. As in Refs. 53 and 61, it is stressed that the current density is spatially uniform throughout the junction in order to satisfy the continuity equation. In the S region one should consider both the current density computed from Eq. (6) and also the integration of the source term in the continuity equation [see Eq. (B2) in the Appendix], since the pair potential is not zero there. To avoid this complexity, we compute the current density from Eq. (6) directly in the F region. Furthermore, we verify that if one includes the contribution from the source term, the current density is indeed uniform across the entire tunneling junctions. From panel (b) of Fig. 6, we find that the current density is maximized at $h_2/E_F = 0.1$. Recalling that the equal-spin triplet correlations f_1 are the most long-ranged at $h_2/E_F = 0.1$, this suggests a correlation between the long-ranged nature of the spin-polarized triplet pairs and the charge transport. Finally, we see that the current density is lowest at $h_2/E_F = 1$, where only one spin band is accessible in both F layers for the current carrying states. The results presented in Fig. 6 therefore strongly suggest that by using relatively thin ferromagnets with weak exchange fields, the half-metallic region will effectively host long-range spin-polarized triplet pairs that offer hints of their signatures in the charge transport behavior. Thus, to achieve these properties for the structures considered here, $h_2/E_F = 0.1$ is the optimal strength for such half-metallic superconducting spintronic devices. We emphasize here that our theoretical results offer a concrete evidence for the generation of triplet current in half-metallic superconducting spin valves and further corroborate experimental results presented in Refs. 9 and 21. If on the other hand it is desired to generate f_1 triplet pairs solely in the superconductor, one should incorporate half-metals into both F regions.

B. Half-Metallic Josephson Junctions

In this subsection we present our results for half-metallic $SF_1F_2F_3S$ Josephson junctions. A diagram of the setup is shown in Fig. 7. A trilayer magnetic configuration is considered to allow for the generation of singlet and triplet correlations by using relatively weak and thin magnets adjacent to the half-metallic layers. This setup creates and effective combi-

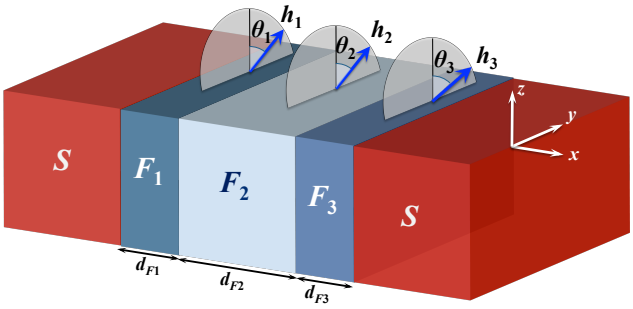

FIG. 7. (Color online) Schematic of the $SF_1F_2F_3S$ Josephson junction. The layers are translationally invariant and extend to infinity in the yz plane. The central F_2 layer is half-metallic ($h_2 = E_F$), while the surrounding F_1 and F_3 layers are ferromagnets with weaker exchange fields $h_1 = h_3 = 0.1E_F$. The angles θ_1, θ_2, and θ_3 describe the angles that the magnetic exchange field vector makes with the z axis in the corresponding F_1, F_2 and F_3 layers with thicknesses d_{F1}, d_{F2}, and d_{F3}, respectively.

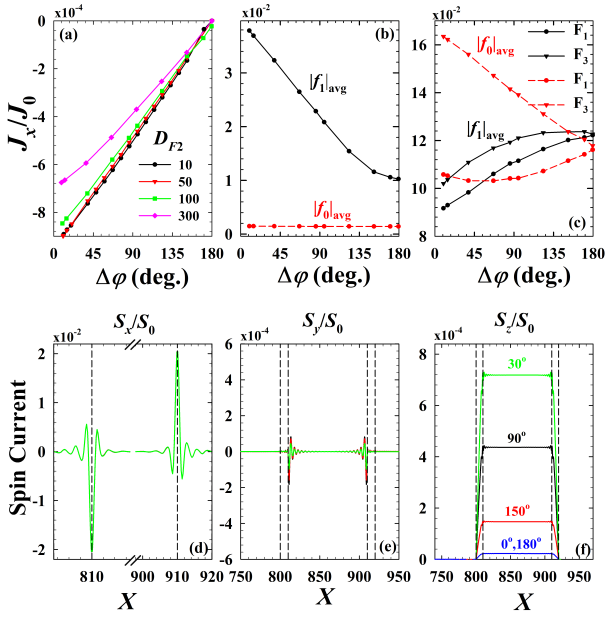

FIG. 8. (Color online) First row (a)-(c): The normalized current density J_x v.s. the phase difference $\Delta\varphi$ for (a) several normalized half-metal thicknesses $D_{F2} = k_F d_{F2}$. (b) The equal-spin f_0 and opposite-spin f_1 triplet correlations spatially averaged over the half metal region F_2, and (c) over the ferromagnetic F_1 and F_3 regions. Second row (d)-(f): The components of the normalized spin current $\boldsymbol{S}$ as a function of dimensionless position $X = k_F x$. In (a)-(f), the exchange fields in F_1 and F_3 are aligned along the y direction, and along z in the half-metal F_2 (see Fig. 7). The ferromagnets F_1 and F_2 have equal thicknesses of $10/k_F$. In panels (b)-(f) the F_2 thickness is fixed at $100/k_F$.

nation of spin-mixing and breaking of spin rotation symmetry, both necessary ingredients for the existence of a Josephson current[35]. For the half-metal thicknesses considered here, a simpler bilayer junction consisting of a thick half-metal and weaker ferromagnet would result in the destruction of phase coherence between the S banks. Two relatively weak ferromagnets are needed to be in contact with the superconductors to effectively generate triplet correlations and establish both charge and spin currents within the junction. For a nonuniform magnetization in the half-metal, there would be a modification to the Andreev reflection amplitudes[67] and corresponding Josephson current. The thicknesses of the S layers are $800/k_F$, while F_1, F_2, and F_3 can vary, depending on the quantity being studied. As before, the superconducting coherence length is fixed to be $100/k_F$. For most cases, the interfaces are generally assumed to be transparent, although cases with interface scattering will be considered as well. Unless otherwise noted, the central F layer is half-metallic, with exchange field corresponding to $h_2 = E_F$. Similar to what was shown for tunnel junctions, the spin-valve effect is maximized when the exchange fields of F_1 and F_3 are weaker: We consider here $h_1 = h_3 = 0.1E_F$. For these Josephson structures, the focus of the investigation is on the influence that the macroscopic phase difference $\Delta\varphi$, and the relative magnetization orientations have on the spin currents, charge currents, and associated triplet correlations. The charge currents are normalized by J_0, where $J_0 = en_e v_F$, and $v_F = k_F/m$ is the Fermi velocity. All three components of the spin current $\boldsymbol{S}$ are normalized similarly[53].

We begin with the self-consistent current phase relation for the $SF_1F_2F_3S$ structure shown in Fig. 7. In Fig. 8(a), the normalized charge current flowing in the x direction, J_x, is shown as a function of the macroscopic phase difference $\Delta\varphi$. The central half-metallic F_2 layer is sandwiched between two weaker ferromagnets with normalized exchange field strengths $h/E_F = 0.1$, and thicknesses $10/k_F$. This type of configuration ensures the necessary singlet-triplet conversion takes place near the superconductors[7]. Each of the ferromagnets F_1 and F_3 have their magnetizations oriented in the same direction (along y) but orthogonal to F_2 (along z). To isolate the triplet spin current flowing through the half-metal, differing dimensionless thicknesses $D_{F2} = k_F d_{F2}$ are considered, as shown in the legend. As seen, the supercurrent essentially obeys a linear trend with phase difference that is weakly dependent on the thickness of the half-metal. As this thickness increases, the current begins to deviate from the linear behavior, as seen developing for the $D_{F2} = 300$ case. The fact that increasing the thickness D_{F2} has a weak effect on the supercurrent reflects the spin-polarized nature of the triplet pairs involved in transport through the half-metal. For a Josephson junction with a half-metallic junction region and spin-flip scattering at the interfaces, a non-self-consistent treatment showed a similar slow decline of the supercurrent as the junction width increases[37]. On the other hand, the presence of impurities can result in an exponential suppression of the supercurrent[35]. The range of the current phase relation in the figure is limited for clarity, and extending the range of $\Delta\varphi$ would result in a sawtooth-like profile with vanishing current at $\Delta\varphi = n\pi$, where is n is an integer. Physically, the slow decay of the equal-spin triplet correlations in the half metal

equates to propagation lengths of the quasiparticles that can well exceed ξ_F. The presence of superconducting correlations deep within half-metals has been experimentally observed in the form of McMillan-Rowell conductance oscillations[19]. A long-ranged supercurrent has also been measured in half-metallic CrO_2 junctions, indicative of the presence of triplet correlations[11]. To demonstrate the slow decay of the equal-spin triplet correlations, in (b) the magnitude of the equal spin correlations f_1 averaged over the half-metallic region F_2 are shown. For comparison, the opposite spin correlations f_0 are also shown. To satisfy the Pauli principle, these spatially symmetric triplet pairing correlations must be odd in time (or frequency), and hence vanish when the relative time t is zero. For half-metallic junctions, the *even*-frequency triplet p-wave component can play a non-negligible role in the Josephson current[50]. For the results involving triplet pairs in this section, we take the corresponding dimensionless time to be $\omega_D t = 4$. Due to the presence of only one spin band in F_2, the f_0 correlations have a very weak extent within the half-metal and remain relatively constant for all $\Delta\varphi$. On the other hand, the f_1 component has a relatively large presence in F_2, increasing as the magnitude of the current increases. In the absence of current, the triplet amplitudes populate the half-metal, consistent with what is found in half-metallic spin valves[75]. As mentioned earlier, the presence of the thin ferromagnet layers is important for the generation of the opposite-spin triplet pairs, and consequently the conversion to the equal-spin channel. This effect is clearly seen in (c), where now the magnitude of the triplet correlations are presented averaged over the F_1 and F_3 layers. As the macroscopic phase difference changes, it is evident that a nontrivial intermixture of f_0 and f_1 occurs in those layers.

In the bottom row of panels ((d)-(f)), the three components of the normalized spin currents are shown as a function of the dimensionless position $X = k_F x$. All components of the spin current flow in the x direction. The dashed vertical lines serve to identify the narrow ferromagnetic regions containing F_1 and F_3. If the F layers possessed uniform magnetization, there would be no net spin current. The introduction of an inhomogeneous magnetization however results in a net spin current imbalance that is finite even in the absence of a Josephson current. In (d), we present the normalized x component of the spin-current, S_x, which is responsible for the torque that tends to align the magnetizations in the ferromagnetic layers. This exchange field mediated effect is present in the absence of Josephson current and is seen to be almost independent of the phase difference that drives the Josephson current. As seen, this quantity is maximized at the interfaces, before undergoing damped oscillations. For completeness, we have included in (e) the y component of the spin current, which for our magnetic configuration is clearly negligible. In panel (f), we examine the normalized z-component of the spin current S_z. This component, which is oriented parallel to the interfaces tends to build up on the weakly ferromagnetic layers and then propagate uniformly in the half-metal. The magnitude of S_z is seen to correlate with the magnitude of the charge current in (a), where the smaller phase differences result in large charge and spin currents that decline as $\Delta\varphi$ increases. These results

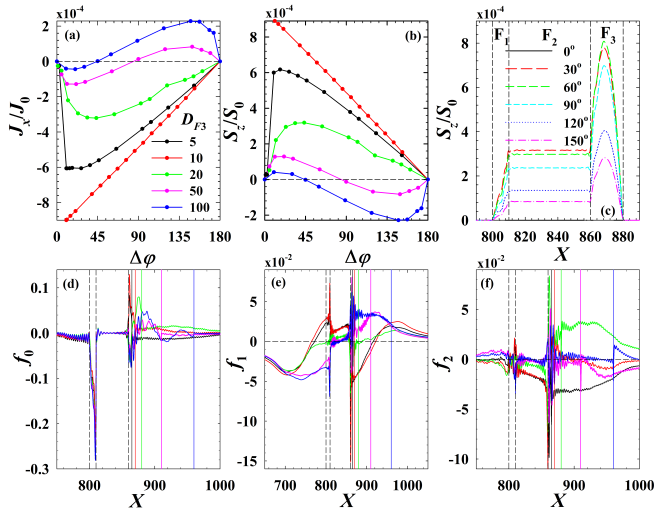

FIG. 9. (Color online) Top row: (a) The normalized charge current density J_x v.s. the phase difference $\Delta\varphi$, (b) the z component of the normalized spin current density S_z within the half-metal region v.s. $\Delta\varphi$ for several D_{F3}, and (c) the normalized S_z as a function of dimensionless position $X \equiv k_F x$ for $D_{F3} = 20$. The legend in (c) labels the different phase differences $\Delta\varphi$ (in degrees) between the S banks. The legend in (a) depicts the ferromagnet thicknesses D_{F3} used in (a), (b), and (d)-(f). Bottom row: The spatial behavior of the real part of the triplet correlations for various thicknesses (see legend in (a)) and for a phase difference of $\Delta\varphi = 90°$. The dashed vertical lines identify the F_1 and F_2 regions located within $800 \leq X \leq 810$ and $810 < X \leq 860$ respectively, while the solid vertical lines mark the various F_3/S interfaces. The exchange field in F_1 and F_3 is aligned along the y direction, while it points along z in the half-metal (see Fig. 7). The thicknesses d_{F1}, and d_{F2} are maintained at the constant dimensionless values of $D_{F1} = 10$ and $D_{F2} = 50$, respectively.

indicate that the half-metal polarizes the spin current along its magnetization direction, and that the Josephson current is due to the propagation of equal-spin triplet pairs.

Next, in Fig. 9(a) the half metal F_2 and ferromagnet F_1 have fixed thicknesses corresponding to $D_{F2} = 50$ and $D_{F1} = 10$, respectively. The ferromagnet F_3 is allowed to vary, as shown in the legend. Asymmetric structures with unequal thicknesses of the ferromagnetic layers has been shown to enhance spin mixing effects that results in the generation of long-ranged spin-polarized triplet pairs[76]. The linear behavior of the charge current previously shown in Fig. 8 where the two magnets F_1 and F_3 are of equal thickness is seen to transition to a sinusoidal-like structure as the difference in the thicknesses between F_1 and F_3 increases. Thus, for highly asymmetric structures, the current phase relation reveals a sign change in the charge current for phase differences between 0° and 180°. Deviations from the sinusoidal current phase relation can also arise in half-metallic Josephson junctions with strong spin-flip interface scattering[15]. The ferromagnet F_3 with relatively weak exchange field compared with F_2 and somewhat larger thicknesses ($D_{F3} = 10$) creates ideal conditions for the creation and propagation of opposite-spin triplet pairs. The center of mass momentum of a given pair

shifts in the presence of spin splitting from the exchange field, resulting in the observed damped oscillations for a given $\Delta\varphi$.

If we now calculate the z component of the spin current flowing through the half-metal portion of the junction, we find that aside from a sign difference, it is nearly identical to the Josephson current as seen in Fig. 9(b). This reaffirms that the current flowing through the half-metal is comprised of Cooper pairs that are polarized in the z direction by the half-metal. In general, the spin current is a non-conserved quantity, in contrast to the charge current. Thus, although S_z is uniform throughout the half-metal, it spatially varies in the other junction regions. This is demonstrated in (c) for several phase differences $\Delta\varphi$ (see legend), where $D_{F1} = 10$, $D_{F2} = 50$, and $D_{F3} = 20$. The spin current does not flow in the outer superconductor banks, and thus S_z increases from zero at the S/F_1 interface ($X = 800$) before reaching its uniform value in the half metal, and then peaks within F_3 before declining to zero again in the superconductor.

To reveal the relative population of triplet pairs throughout the junction, we consider in (d)-(f) the triplet correlations f_0, f_1, and f_2, as functions of normalized position X. The phase difference is set according to $\Delta\varphi = 90°$. We still have $D_{F1} = 10$, and $D_{F2} = 50$, but several D_{F3} are shown with values given in the legend found in panel (a), thus creating a broad range of current profiles. The opposite-spin triplet correlations shown in (d) reveal that f_0 spikes in the F_1 region, weakly dependent on D_{F3}. Within F_2 however, the single spin band present in the half-metal severely diminishes f_0. When F_3 has thin layers, the greater confinement enhances the f_0 amplitudes. Increasing D_{F3} eventually provides sufficient space for the exchange field to induce damped oscillations of the opposite-spin pairs. Thus, although it is energetically unfavorable for the f_0 correlations to reside in the half metal, they do become enhanced in the surrounding ferromagnets when they are thin ($D_{F3} = 5, 10$). Under these conditions, the spin polarized triplet pairs f_1 and f_2 propagate within the half metallic region, as seen in (e) and (f). It is also evident that often the equal-spin triplets do not decay within the S regions, but rather extend deep into the superconductor banks.

Having seen the influence that the layer thicknesses in half-metallic Josephson junctions have on the charge and spin currents, we now turn to the the effects of magnetization rotations. Rotating the magnetization in one of the junction layers can be achieved experimentally via external magnetic fields, or spin-torque switching. In Fig. 10(a) we display the magnitude of the normalized charge current as a function of the magnetization angle θ_1. The half metal thickness is set at $D_{F2} = 50$, and the surrounding ferromagnets have equal thicknesses of $D_{F1} = D_{F3} = 10$. The effects of scattering at the S/F_1 and F_3/S interfaces are accounted for by setting the dimensionless parameter $H_{B1} \equiv H_1/v_F = 0.8$ and $H_{B4} \equiv H_4/v_F = 0.8$, respectively. Here H_1 and H_4 are the delta-function scattering strengths at those two interfaces[53]. If nonmagnetic impurities are present at the interfaces, there can be an enhancement of the Andreev reflection processes, leading to an increase of the Josephson current[68]. The inclusion of interfacial scattering however, generally tends to suppress the linear sawtooth profile in the current phase relation[53].

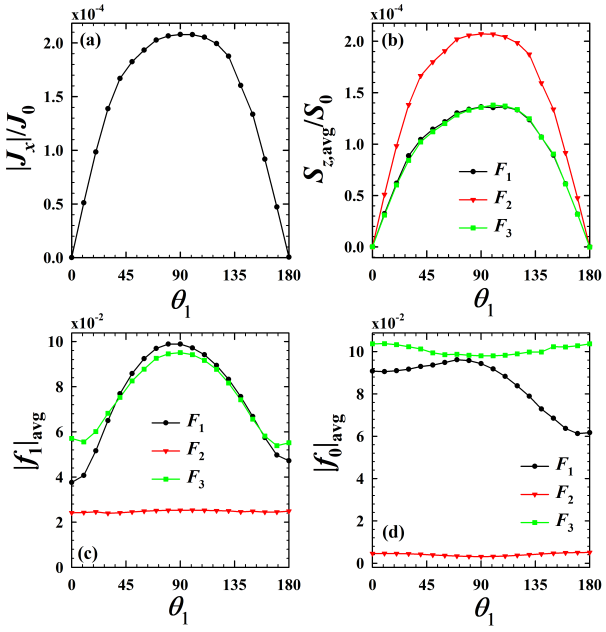

FIG. 10. (Color online) Top row: (a) Normalized charge currents and (b) the z component of normalized spin currents in each junction region as a function of the magnetization alignment angle θ_1. Bottom row: Spatially averaged equal-spin (c) and opposite-spin (d) triplet correlations as a function of θ_1. The thicknesses of F_1, F_2, and F_3 are set to be $10/k_F$, $50/k_F$, and $10/k_F$, respectively. An interface scattering strength of $H_{1,4} = 0.8$ is present at the interfaces (see main text), and a phase difference of $\Delta\varphi = 90°$ is assumed.

The Josephson current is established with a phase difference $\Delta\varphi = 90°$ between the superconducting banks. The half metal layer has its ferromagnetic exchange field directed along z and for F_3, it is directed along y (see Fig. 7). Thus, when $\theta_1 = 0°$ or $\theta_1 = 180°$, both F_1 and the adjacent half metallic layer have magnetizations that are parallel or antiparallel, respectively. At these points, J_x vanishes while the supercurrent flow is largest when $\theta_1 = 90°$, corresponding to when the junction layers have magnetizations that are orthogonal to one another, and hence possess a high degree of magnetic inhomogeneity. Similarly, manipulation of the supercurrent through relative variations of $\Delta\varphi$ and the magnetization angles was also exhibited using a non-self-consistent scattering approach[66]. The half-metal tends to align the spin of any entering quasiparticles along the z direction, and this component of the normalized spin current displays essentially identical behavior to J_x as seen in (b). The averaged spin current is distributed equally throughout the two outer ferromagnets, but weaker overall since it must vanish at the boundaries with the superconductors. In previous work[14] an S-matrix quasiclassical theory was developed for half-metallic Josephson junctions with spin active interfaces, showing that the supercurrent has to be carried by the equal-spin triplet pairs. The behavior of the magnitudes of the triplet correlations v.s. θ_1 is presented in panels (c) and (d). When $\theta_1 = 0°$ or $\theta_1 = 180°$, the generation of equal-spin triplets are suppressed in the ferromagnets

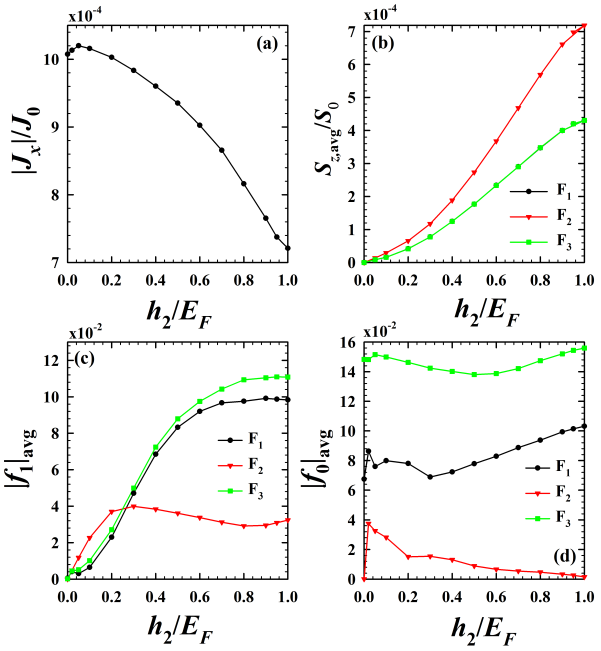

FIG. 11. (Color online) Top row: Normalized charge current (a) and average spin currents (b) v.s. the dimensionless magnetization strength h_2/E_F. Bottom row: Spatially averaged equal-spin (c) and opposite-spin (d) triplet correlations as a function of h_2/E_F. The thicknesses of F_1, F_2, and F_3 are set to be $10/k_F$, $100/k_F$, and $10/k_F$, respectively. The legend in (b) identifies each region of the junction in which the quantities in (b)-(d) are averaged over. Here, transparent interfaces are considered and $\Delta\varphi = 30°$.

F_1 and F_3 due to the lowering of the overall magnetic inhomogeneity. For these situations, the magnetizations in the F_1 and F_2 layers are collinear, however, f_1 does not vanish due to the orthogonal magnetization in F_3. On the contrary, when $\theta_1 = 90°$, the magnetization in each ferromagnet is orthogonal to the adjacent one, resulting in favorable conditions for the creation of the equal spin triplets. In (d) the importance of having relatively weak and thin outer ferromagnets for the triplet conversion process is exhibited by the population of the f_0 triplet components in those regions.

It was observed that the presence of the half-metal in the junction serves to filter out the opposite-spin triplet pairs, creating a platform in which to study spin polarized triplet correlations. It is of interest to clarify the role that the exchange field strength in the half metal region has on the charge and spin transport. The top row of Fig. 11 therefore shows the magnitude of the charge current and the averaged spin current, both normalized, as a function of the exchange field strength in the half metal, h_2. The phase difference is set to $\Delta\varphi = 30°$. For clarity, the two ferromagnets have equal thicknesses, $D_{F1} = D_{F3} = 10$, and there is no interface scattering present. The larger half metal has a thickness of $D_{F2} = 100$, and the exchange field varies from $h_2 = 0$ to $h_2 = E_F$, which coincides with a nonmagnetic normal metal and a half-metallic phase, respectively. The junction's magnetization profile is in an optimal inhomogenous state, with alignment angles are as follows: $\theta_1 = 90°$, $\theta_2 = 0°$, and $\theta_3 = 90°$, corresponding to magnetization alignments along y, z, and y, respectively. Examining panel (a), it is evident that the magnitude of the charge current J_x is maximal when the F_2 layer is weakly ferromagnetic, and is minimal when F_2 is half-metallic. When only one electrode is present, it was shown that the current is optimized for intermediate exchange field strengths and vanishes in the half-metallic limit[51]. The spatially averaged spin current on the other hand is anticorrelated with J_x, as it monotonically increases with larger exchange fields. Indeed, S_z vanishes when the central F_2 layer is a nonmagnetic normal metal, and peaks when it is half-metallic. When the central layer is nonmagnetic S_z vanishes since the only active magnetic layers in this case are F_1 and F_3 which have parallel magnetization directions. Examining the bottom row, the triplet correlations are also shown averaged over each of the three junction layers. In (c) the magnitude of the f_1 correlations are shown v.s. h_2/E_F. When $h_2 = 0$, F_1 and F_3 are the only ferromagnetic layers in the junction, and their magnetizations are oriented along y. Since they are collinear, spin-polarized triplet pairs cannot be generated, and hence $f_1 = 0$. Increasing h_2 and hence the degree of polarization in the F_2 layer continuously increases the amount of spin polarized triplet pairs in the ferromagnets F_1 and F_3, with f_1 largest when F_2 is half-metallic. This is consistent with the experimental observation of enhanced spin valve effects arising from the increased generation of f_1 correlations in a half-metal[21]. The f_1 correlations in F_2 also become enhanced as its exchange field get larger, until $h_2/E_F \approx 0.3$. Further increases in h_2 result in a slight decline before ultimately increasing again as F_2 approaches the half-metallic limit. This demonstrates the importance of using a highly spin-polarized material in the central junction region to optimize triplet pair generation in each layer. The opposite-spin pairs f_0 are also maximized in the triplet conversion layers F_1 and F_3 when $h_2 = E_F$ as seen in (d). Unlike what is found for f_1, the f_0 correlations are not constrained to vanish when $h_2 = 0$ since they can exist when the ferromagnets have collinear magnetizations. Thus the thin ferromagnetic regions have a substantial portion of f_0 pairs when $h_2 = 0$. Within the thicker F_2 layer however, f_0 is significantly reduced overall, becoming negligibly small in the nonmagnetic metal ($h_2 = 0$) and half-metallic ($h_2 = E_F$) limits. This substantiates the idea that using a half-metal for F_2 enables one to focus on the interplay between the spin current and the equal spin pairs f_1 in the F_2 region.

We now take the structure previously studied above in Fig. 11 and incorporate interface scattering, and rotate the magnetizations so that they are interchanged for the first two layers. Thus, F_1 and F_2 have their magnetizations aligned along the z and y axes respectively. The normalized interface scattering strength is set at $H_1 = H_4 = 0.8$. With these parameters, Fig. 12 examines the normalized Josephson supercurrent as a function of the phase difference $\Delta\varphi$. Three magnetization orientations for F_3 are investigated for each of the three panels: $\theta_3 = 0, 90°$, and $180°$ (corresponding to the z, y, and $-z$ directions, respectively). The supercurrent reveals that, depending on whether the magnetization in F_3 is collinear or orthogonal to the adjacent half-metal, the direc-

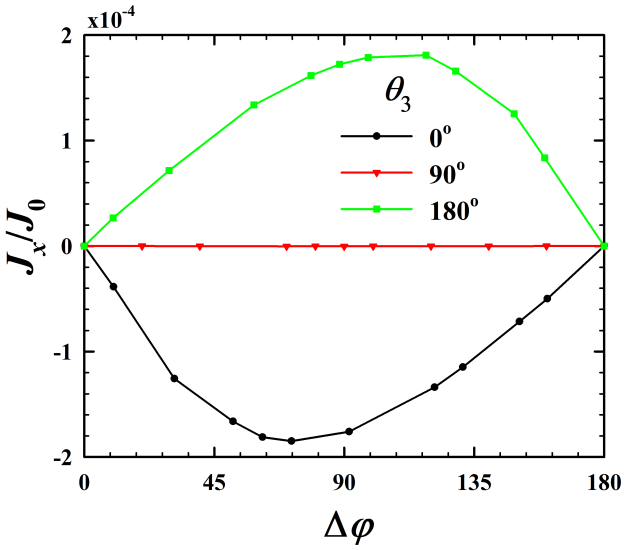

FIG. 12. (Color online) Charge current as a function of phase difference $\Delta\varphi$. The thicknesses of F_1, F_2, and F_3 are set to be $10/k_F$, $100/k_F$, and $10/k_F$, respectively. The interface scattering strengths are set to $H_{B1} = H_{B4} = 0.8$. The magnetization in F_1 and F_2 is along the z and y directions respectively. In the ferromagnet F_3, the magnetization orientation angles θ_3 varies as shown ($\theta_3 = 0$ is along z, $\theta_3 = 90°$ is along y, and $\theta_3 = 180°$ is along -z).

tion of the charge current can be reversed or turned off completely. When $\theta_3 = 0$, the magnetization in each layer is orthogonal to one another, and the current phase relation reveals that when starting from zero phase difference, the magnitude of the current increases until $\Delta\varphi \approx 70°$, before declining back to zero again at $\Delta\varphi = 180°$. Due to quasiparticle scattering that takes place at the interfaces, the coherent transport of Cooper pairs through the junction is significantly altered compared to when the interfaces were transparent, resulting in the observed overall reduction in current and deviation from the previous linear behavior found in Fig. 8. Previously, when studying how magnetization rotation affected the charge current in Fig. 10(a), we found that when two adjacent layers in the junction have collinear magnetizations, the charge current vanished. This is consistent with Fig. 12, where the current vanishes for all phase differences at $\theta_3 = 90°$. Rotating the magnetization further to $\theta_3 = 180°$, the magnetizations in both ferromagnets are orthogonal to the half-metal, as in the $\theta_3 = 0$ case, but antiparallel to each other. This causes a reversal of the charge current as shown.

As shown earlier, the charge current that flows due to the macroscopic phase differences between the S electrodes can become spin-polarized when entering one of the ferromagnetic or half-metal layers. This spin current can then interact with the other ferromagnets and become modified by the corresponding magnetizations. Having established in Fig. 12 how the charge current can be manipulated for a half-metallic Josephson junction, it is important to next identify how the spin currents behave in each layer, as control of these spin currents is vital for spintronic applications. It has been shown that within a quasiclassical formalism, spin supercurrents can flow in the absence of a charge current[51]. To explore the spin currents using our self-consistent, microscopic approach, Fig. 13 shows the phase dependence for the spatially averaged spin current $\boldsymbol{S}$. We implement the same experimentally accessible parameters used in Fig. 12. Each row of three panels corresponds to one of the three magnetization orientations θ_3 (as labeled). As discussed earlier, the central half-metallic layer maintains a constant spin current, that can couple the surrounding ferromagnets F_1 and F_3. This effect is evident for S_x when $\theta_3 = 0°$ (top row), corresponding to the z,y,z magnetic configuration for the respective F_1, F_2, and F_3 layers. This spin current component, normal to the interfaces, is essentially the static contribution to the spin current, which participates in spin-transfer torque effects near the ferromagnet/half-metal interfaces where misaligned exchange fields are present. Thus, S_x varies in space, resulting in a local STT [recall $\partial S_x/\partial x = \tau_x$] that tends to rotate the corresponding magnetizations in opposite directions. Within the half-metal, the spin current oscillates as it damps out deep within F_2, resulting in an average S_x of zero, as exhibited in (a). The averaged spin currents clearly do not depend on the phase difference, as expected for a static effect. The strong influence of the half-metal is exhibited by S_y, the spin current component that lies in the same direction as the exchange field in the half-metal. The half-metal is seen to polarize not only the spin current within it, but also within the surrounding weak magnets whose intrinsic exchange fields are in the orthogonal z direction. Note that the y-component of spin currents in each of the F regions have similar overall behavior as a function of $\Delta\varphi$, with the average S_y being equal in F_1 and F_3, and largest in F_2. Comparing this to Fig. 12, it is clear that apart from a sign difference, the normalized spin current S_y in the half-metal and the supercurrent J_x are nearly identical. This implies that the spin-polarized current S_y in the half-metal correlates with the charge current that is flowing there. Therefore, the charge transport is governed by spin-polarized Cooper pairs corresponding to the equal-spin correlations. Turning now to the middle row, where $\theta_3 = 90°$, there is no spin current along y for all of the F layers. Within the F_3 layer, the normalized S_x is shown to vanish at $\Delta\varphi = 90°$, while S_z is maximal for that phase difference. Considering the phase differences that yield no supercurrent, $\Delta\varphi = 0°$ and $180°$, The spin currents S_x and S_z are seen to be anti-correlated, with S_z now vanishing, and the magnitude of S_x having now become largest in F_3. Finally, the bottom row depicts the spin currents for $\theta_3 = 180°$. As was found for the previous $\theta_3 = 0°$ case, we see a direct correlation between the charge supercurrent [Fig. 12] and the y component of the spin current for this magnetic configuration. The main differences being that the directions of the charge and spin currents are reversed, due to θ_3 having a reversed collinear orientation, and non-vanishing S_x in F_2.

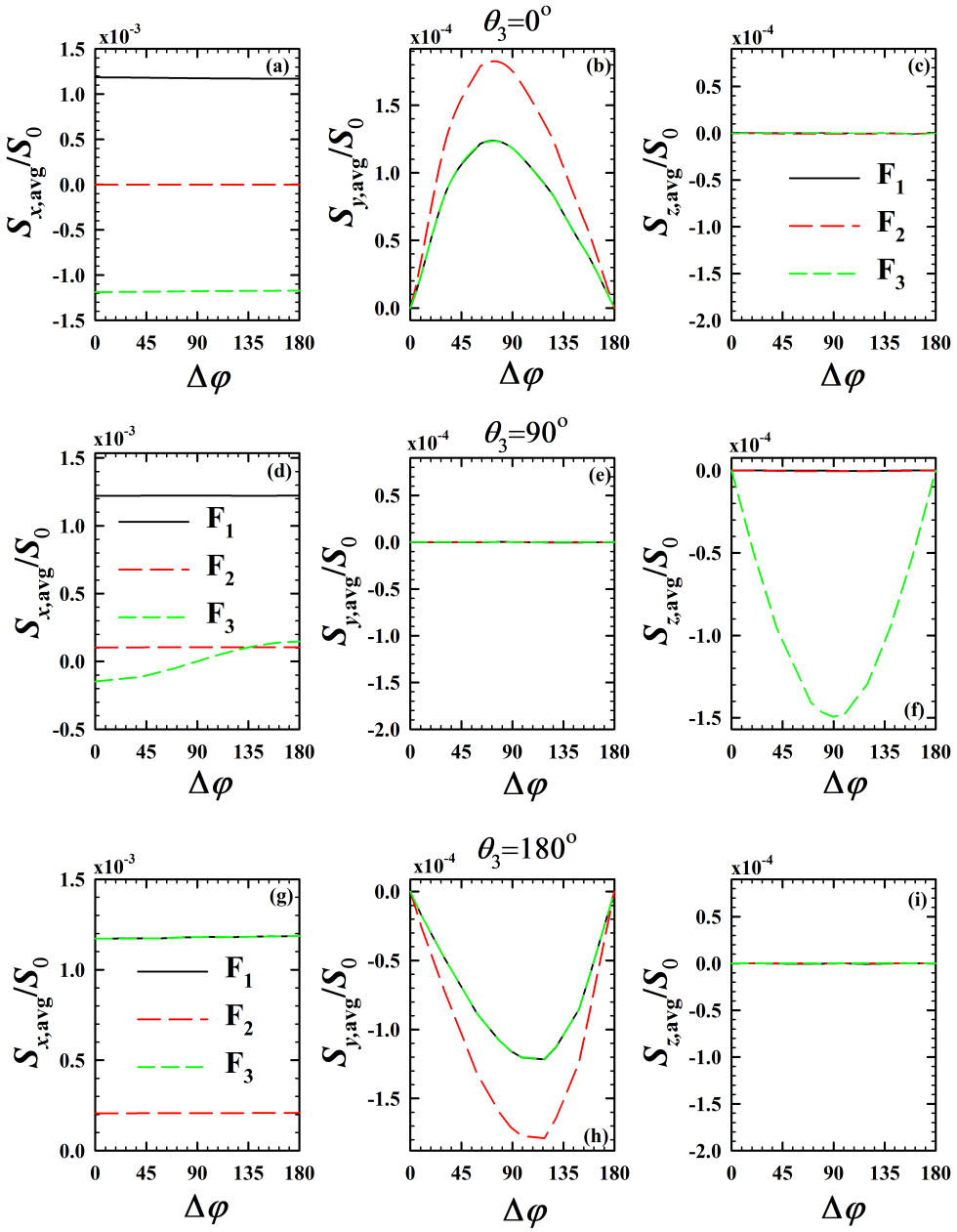

FIG. 13. (Color online) Components of the average spin current in each region v.s. the phase difference $\Delta\varphi$. Three magnetization orientations of the outer ferromagnet F_3 are shown: $\theta_3 = 0$ (top row), $\theta_3 = 90°$ (middle row), and $\theta_3 = 180°$ (bottom row). The thicknesses of F_1, F_2, and F_3 are set to be $10/k_F$, $100/k_F$, and $10/k_F$, respectively. The dimensionless interface scattering strengths correspond to $H_{B1} = H_{B4} = 0.8$.

IV. CONCLUSIONS

In this paper, we have studied in detail the interplay between the triplet pairs and transport properties of half-metallic superconducting spin valves including tunnel junctions and Josephson junctions. In tunnel junctions with the presence of an applied bias voltage, we have discussed a useful theoretical approach combining the self-consistent solutions to the Bogoliubov-de Gennes equations and the transfer matrix method based on the Blonder-Tinkham-Klapwijk formalism. By utilizing this approach, we were able to determine the bias dependence of the spin transport quantities and induced triplet pair amplitudes. We first investigated the bias-induced magnetizations, spin currents, and the spin-transfer torques as functions of position for various misorientation angles between the half metal and adjacent weak ferromagnet. We found that their behaviors can be largely explained by the precessional effect: When the injected charge current spin-polarized by the half-metal enters the weak ferromagnet, its polarization state can be rotated by the local exchange interaction. The bias dependence of these spin transport quantities were also studied.

We find that their magnitudes increase linearly when external bias voltages are larger than the saturated superconducting pair amplitudes. We then showed that the spin transport quantities are determined by two important parameters: the exchange interaction and thickness of the weak ferromagnet. Both $m = 0$ and $m = \pm 1$ triplet correlations of the tunnel junctions were also presented. We found that they are anticorrelated when the misorientation angle between exchange interactions in the ferromagnetic layers is varying. Furthermore, the long-range nature of $m = \pm 1$ triplet correlations in the half-metallic region is established and proven to be important in the half-metallic tunnel junctions. It was shown that by choosing the exchange interaction to be about $0.1E_F$, the spin-valve effect is optimized.

We then turned to the study of half-metallic Josephson junctions, consisting of a half metal sandwiched by two weak ferromagnets in the non-superconducting region. First, we considered a symmetric situation where the thicknesses and exchange fields are the same for the two weak magnets. To generate all components of triplet pairs, the exchange field in the half metal was directed perpendicular to that of the weak magnets. We studied the current phase relations and found that the current was only weakly dependent on the thickness of the half metal indicating that the supercurrent was carried by equal-spin triplet pairs. This was also corroborated by the fact that the charge current was strongly correlated with the spin current as a function of the phase difference between the two superconducting banks. We also investigated the asymmetric situation where the thickness of one of the weak magnets was adjusted. We again found that the equal-spin triplet pairs were responsible for the flow of supercurrent and spin current. Next, we analyzed the effects of changing the angle between the exchange field in the half metal and the adjacent weak magnet. When the misorientation angle was 90°, the charge current, the equal-spin triplet pair amplitudes, and the spin currents attained their maximum values. On the other hand, when the angle was 0° or 180°, both the charge and spin currents vanished, showing the importance of the magnetic configuration in half-metallic Josephson junctions. The induced triplet correlations also depend on the exchange interaction for the central ferromagnet. They saturate when the half-metallic limit is reached. Finally, we showed that when the exchange fields in the weak magnets have the same magnitude and are perpendicular to that of the half metal, the spin-valve effect is most pronounced.

ACKNOWLEDGMENTS

C.-T.W. is supported by the MOST Grant No. 106-2112-M-009-001-MY2, the NCTS of Taiwan, R.O.C. and a grant of HPC resources from NCHC. K.H. is supported in part by ONR and a grant of HPC resources from the DOD HPCMP. K.H. would also like to thank M. Alidoust for useful discussions pertaining to this work.

Appendix A: Transfer Matrix Approach

Here we present the details of how to adopt the transfer matrix approach to extract relevant reflection and transmission amplitudes. If one considers a bilayer tunnel junction that is made up of a non-magnetic metal and a superconductor, then the eigenfunctions in the non-magnetic metallic region are only linear combinations of particle and hole wavefunctions[72]. However, in our work, where the non-magnetic metallic region is replaced by two ferromagnetic layers, one should consider the spin degree of freedom in addition to the particle-hole nature. Because the exchange field is along z in F_1 (see Fig. 1), the appropriate eigenfunctions are

$$\begin{pmatrix} e^{\pm ik^+_{\uparrow 1}x} \\ 0 \\ 0 \\ 0 \end{pmatrix}, \begin{pmatrix} 0 \\ e^{\pm ik^+_{\downarrow 1}x} \\ 0 \\ 0 \end{pmatrix}, \begin{pmatrix} 0 \\ 0 \\ e^{\pm ik^-_{\uparrow 1}x} \\ 0 \end{pmatrix}, \begin{pmatrix} 0 \\ 0 \\ 0 \\ e^{\pm ik^-_{\downarrow 1}x} \end{pmatrix}, \tag{A1}$$

where the subscript 1 denotes the F_1 regions and the superscript + is for particle-like and − is for hole-like wavefunctions. When the eigenenergy ϵ is specified, the corresponding wavevectors are given by the following relation

$$k^{\pm}_{s1} = \left[1 - \eta_s h_1 \pm \epsilon - k^2_\perp\right]^{1/2}, \tag{A2}$$

where $k^2_\perp = k^2_y + k^2_z$. The incident angle, θ_I, relative to the normal of the interface with spin s is related to $k_\perp$ and given by the relation, $\tan\theta_I = k_\perp / k^{\pm}_{s1}$. The reflected angles, θ_R, similarly obey $\tan\theta_R = k_\perp / k^{\pm}_{s1}$. From Eq. (A2), it is easy to see that the reflected angles depend on both the spin as well as whether the quasiparticle is particle-like or hole-like. The exchange field in F_2 lies on the yz plane, and it is tilted relative to the z-axis by the angle θ. One needs again to use suitable eigenfunctions for both particle and hole branches in F_2. The particle-like wavefunction with spin parallel to the exchange field in F_2 and antiparallel to the exchange field in F_2 are given as

$$\begin{pmatrix} \cos(\theta/2) \\ \sin(\theta/2) \\ 0 \\ 0 \end{pmatrix} e^{\pm ik^+_{\uparrow 2}x}, \quad \begin{pmatrix} -\sin(\theta/2) \\ \cos(\theta/2) \\ 0 \\ 0 \end{pmatrix} e^{\pm ik^+_{\downarrow 2}x}, \tag{A3}$$

respectively. Similarly, the hole-like wavefunction with spin parallel and antiparallel to the exchange field in F_2 are given by

$$\begin{pmatrix} 0 \\ 0 \\ \cos(\theta/2) \\ -\sin(\theta/2) \end{pmatrix} e^{\pm ik^-_{\uparrow 2}x}, \quad \begin{pmatrix} 0 \\ 0 \\ \sin(\theta/2) \\ \cos(\theta/2) \end{pmatrix} e^{\pm ik^-_{\downarrow 2}x}, \tag{A4}$$

respectively. Here the momenta are defined through the relation

$$k^{\pm}_{s2} = \left[1 - \eta_s h_2 \pm \epsilon - k^2_\perp\right]^{1/2}. \tag{A5}$$

Note here that following previous conventions, we denote "+" for particles, and " − " for holes. Because the Hamiltonian is

translationally invariant in the yz plane, the perpendicular momentum $k_\perp$ is a constant throughout the "entire" junction for a given eigenstate appropriate to the entire junction. Once the energy of the eigenstate, ϵ, is prescribed, the eigenfunctions in the F_2 region are given as a linear combination of these wavefunctions. Accordingly, there are eight unknowns associated with this linear combination. On the superconducting side, one can easily show that in 4×4 Nambu space, the appropriate wavefunctions are

$$\begin{pmatrix}u_0\\0\\0\\v_0\end{pmatrix}e^{\pm ik^+x},\quad\begin{pmatrix}0\\u_0\\v_0\\0\end{pmatrix}e^{\pm ik^+x},\quad\begin{pmatrix}v_0\\0\\0\\u_0\end{pmatrix}e^{\pm ik^-x},\quad\begin{pmatrix}0\\v_0\\u_0\\0\end{pmatrix}e^{\pm ik^-x},\tag{A6}$$

where $k^\pm = 1 \pm \sqrt{\epsilon^2-\Delta_0^2-k_\perp^2}$. If a non-self-consistent pair potential is adopted for which the pair potential in the S region is a constant, the entire S region is just a linear combination of the above wavefunctions with suitable constants u_0 and v_0 given by,

$$u_0^2 = \frac{1}{2}\left(1+\frac{\sqrt{\epsilon^2-\Delta_0^2}}{\epsilon}\right),\tag{A7a}$$

$$v_0^2 = \frac{1}{2}\left(1-\frac{\sqrt{\epsilon^2-\Delta_0^2}}{\epsilon}\right),\tag{A7b}$$

where Δ_0 is the constant pair amplitude. Let us first discuss the non-self-consistent case and suppose a spin-up particle is sent from an electrode into the F_1 region. In the F_1 region, one needs to include the incident spin-up particle wavefunction as well as four different types of reflection: (1) a reflected particle wavefunction with spin-up, (2) a reflected particle wavefunction with spin-down, (3) an Andreev reflected hole wavefunction with spin-up, and (4) an Andreev reflected hole wavefunction with spin-down. As a result, we have four unknowns associated with these four reflected wavefunctions. In the F_2 region, all eight possibilities, Eqs. (A3) and (A4), must be considered, since in general the waves can travel in either the $+x$ or $-x$ directions. In the S region, there are four different types of transmitted wavefunctions: two transmitted particle-like wavefunctions,

$$\begin{pmatrix}u_0\\0\\0\\v_0\end{pmatrix}e^{ik^+x},\quad\begin{pmatrix}0\\u_0\\v_0\\0\end{pmatrix}e^{ik^+x},\tag{A8}$$

and two transmitted hole-like wavefunctions,

$$\begin{pmatrix}v_0\\0\\0\\u_0\end{pmatrix}e^{-ik^-x},\quad\begin{pmatrix}0\\v_0\\u_0\\0\end{pmatrix}e^{-ik^-x}.\tag{A9}$$

Thus, the total number of unknowns in this process is sixteen (four from the reflections, eight associated with the F_2 region, and four from the transmissions). We have exactly the same number of constraints to solve for these unknowns because there are two interfaces (F_1/F_2 and F_2/S) at which the continuous conditions of the wavefunction and its derivative must hold when the interfacial barrier is absent.

If one uses a self-consistent profile for the pair amplitude, Δ is not a constant and it varies with x. It is convenient to consider a transfer-matrix approach to take into account the variation of Δ. The details of this approach are presented in Ref. 61 and will not be repeated in this paper. Here, we only summarize the outline of this approach. One first divides the S region into a number of small subregions and approximates each subregion by a constant potential. One can then write down suitable wavefunctions in each subregion. Except for the last subregion where there are only four unknowns linked to four types of transmission, there are eight unknowns associated with each subregion, resulting now in an overall greater number of unknowns. By recognizing the fact that unknowns on one side of an interface are related to those on the other side, we can write,

$$\tilde{\mathcal{M}}_i x_i = \mathcal{M}_{i+1}x_{i+1},\tag{A10}$$

where i is the index of each subregion, $\tilde{\mathcal{M}}_i$ and $\mathcal{M}_{i+1}$ are the corresponding matrices determined by matching the boundary conditions, and x_i and x_{i+1} are the column vectors composed of the unknowns in the i-th and $i+1$-th subregions. By using this recurrence relation, one naturally relates the reflection coefficients in the F_1 region with the transmission coefficients in the outermost S layer. Once these transmission and reflection coefficients are found, they can be fed back into the recurrence relation to generate solutions in each subregion. The transfer matrix method is advantageous because the size of the matrix equation needed to be solved is much smaller than the number of unknowns, albeit at the cost of multiplying matrices.

Appendix B: Charge and Spin Transport

From the Heisenberg equation for the charge density $\rho(\boldsymbol{r})$,

$$\frac{\partial}{\partial t}\langle\rho(\boldsymbol{r})\rangle = i\left\langle\left[\mathcal{H}_{eff},\rho(\boldsymbol{r})\right]\right\rangle,\tag{B1}$$

it is not difficult to obtain the following continuity condition for the current density $\boldsymbol{J}$:

$$\frac{\partial}{\partial t}\langle\rho(\boldsymbol{r})\rangle + \nabla\cdot\boldsymbol{J} = -4e\mathrm{Im}\left[\Delta(\boldsymbol{r})\left\langle\psi_\uparrow^\dagger(\boldsymbol{r})\psi_\downarrow^\dagger(\boldsymbol{r})\right\rangle\right].\tag{B2}$$

When in the steady state, the first term on the left is dropped. Moreover, when the system is in equilibrium without an external bias, one can use the Bogoliubov transformation together with the conservation law for our quasi-one-dimensional system to conveniently write the continuity equation as:

$$\frac{\partial J_x(x)}{\partial x} = 2e\mathrm{Im}\left\{\Delta(x)\sum_n\left[u_{n\uparrow}^*v_{n\downarrow}+u_{n\downarrow}^*v_{n\uparrow}\right]\tanh\left(\frac{\epsilon_n}{2T}\right)\right\}.\tag{B3}$$

The self-consistency condition, Eq. (3), demands that the right hand side of Eq. (B3) vanishes and that the current is a constant throughout the junction, as expected.

Using again the Heisenberg equation can give the proper conservation law[61,77] for spin densities:

$$\frac{\partial}{\partial t}\langle \boldsymbol{\eta}(\boldsymbol{r},t)\rangle = i\langle[\mathcal{H},\boldsymbol{\eta}(\boldsymbol{r},t)]\rangle. \tag{B4}$$

After carrying out some lengthy algebra, we obtain the desired continuity equation,

$$\frac{\partial}{\partial t}\langle \boldsymbol{\eta}(\boldsymbol{r},t)\rangle + \frac{\partial \boldsymbol{S}}{\partial x} = \boldsymbol{\tau}, \tag{B5}$$

where $\boldsymbol{S}$ is the spin current and $\boldsymbol{\tau}$ is the associated spin-transfer torque. They are given by

$$\boldsymbol{S} = \frac{i\mu_B}{2m}\sum_s \left\langle \psi_s^\dagger \boldsymbol{\sigma}\frac{\partial \psi_s}{\partial x} - \frac{\partial \psi_s^\dagger}{\partial x}\boldsymbol{\sigma}\psi_s \right\rangle, \tag{B6}$$

$$\boldsymbol{\tau} = 2\sum_{ss'}\langle \psi_s^\dagger(\boldsymbol{r})\,(\boldsymbol{\sigma}\times\boldsymbol{h})_{ss'}\,\psi_{s'}(\boldsymbol{r})\rangle = 2\boldsymbol{m}\times\boldsymbol{h}. \tag{B7}$$

Appendix C: Spin Rotations

Here we outline the spin rotations that are performed on the triplet components (f_0, f_1, f_2) in Eq. (10). By aligning the spin axes with the local exchange field directions, the role of the triplet correlations and their physical interpretation becomes clearer. The central quantity that we use to perform the desired rotations is the spin transformation matrix $\mathcal{T}$ in particle-hole space. The quasiparticle amplitudes transform as,

$$\Psi'_n(x) = \mathcal{T}\Psi_n(x), \tag{C1}$$

where $\Psi_n(x) = (u_{n\uparrow}(x), u_{n\downarrow}(x), v_{n\uparrow}(x), v_{n\downarrow}(x))$, and the prime denotes quantities in the rotated system. The matrix $\mathcal{T}$ can be written solely in terms of the angles that describe the local magnetization orientation. In particular, when the orientation of the exchange fields in a given layer is expressed in terms of the angles given in Eq. (7), we can write:

$$\mathcal{T} = \begin{bmatrix} \cos(\theta_i/2) & -i\sin(\theta_i/2) & 0 & 0 \\ -i\sin(\theta_i/2) & \cos(\theta_i/2) & 0 & 0 \\ 0 & 0 & \cos(\theta_i/2) & -i\sin(\theta_i/2) \\ 0 & 0 & -i\sin(\theta_i/2) & \cos(\theta_i/2) \end{bmatrix}. \tag{C2}$$

Using the spin rotation matrix $\mathcal{T}$, it is also possible to transform the original BdG equations $\mathcal{H}\Psi_n = \epsilon_n\Psi_n$ (Eq. (2)) by performing the unitary transformation: $\mathcal{H}' = \mathcal{T}\mathcal{H}\mathcal{T}^{-1}$, with $\mathcal{T}^\dagger\mathcal{T} = 1$. As is the case under all unitary transformations, the eigenvalues here are preserved, but the eigenvectors are modified in general according to Eq. (C1). Thus we can write,

$$u'_{n\uparrow} = \cos(\theta_i/2)\,u_{n\uparrow} - i\sin(\theta_i/2)u_{n\downarrow}, \tag{C3}$$
$$u'_{n\downarrow} = \cos(\theta_i/2)\,u_{n\downarrow} - i\sin(\theta_i/2)u_{n\uparrow}, \tag{C4}$$
$$v'_{n\uparrow} = \cos(\theta_i/2)\,v_{n\uparrow} - i\sin(\theta_i/2)v_{n\downarrow}, \tag{C5}$$
$$v'_{n\downarrow} = \cos(\theta_i/2)\,v_{n\downarrow} - i\sin(\theta_i/2)v_{n\uparrow}. \tag{C6}$$

The terms involved in calculating the singlet pair correlations (Eq. (3)), thus obey the following relation between the transformed (primed) and untransformed quantities:

$$u'_{n\uparrow}v'^*_{n\downarrow} + u'_{n\downarrow}v'^*_{n\uparrow} = u_{n\uparrow}v^*_{n\downarrow} + u_{n\downarrow}v^*_{n\uparrow}. \tag{C7}$$

Therefore the terms that dictate the singlet pairing are invariant for any choice of quantization axis, transforming as scalars under spin rotations.

The terms governing the triplet amplitudes on the other hand are in general not invariant under spin-rotations. The relevant particle-hole products in Eq. (10a) that determine f_0, upon the spin transformations obey the following relationships:

$$\begin{aligned} u'_{n\uparrow}v'^*_{n\downarrow} - u'_{n\downarrow}v'^*_{n\uparrow} &= \cos\theta_i(u_{n\uparrow}v^*_{n\downarrow} - u_{n\downarrow}v^*_{n\uparrow}) \\ &\quad + i\sin\theta_i\left(u_{n\uparrow}v^*_{n\uparrow} - u_{n\downarrow}v^*_{n\downarrow}\right), \\ &= f_0\cos\theta_i + i\sin\theta_i f_2, \end{aligned} \tag{C8}$$

For the equal-spin component f_1 [Eq. (10b)], the rotation leaves f'_1 unchanged:

$$u'_{n\uparrow}v'^*_{n\uparrow} + u'_{n\downarrow}v'^*_{n\downarrow} = u_{n\uparrow}v^*_{n\uparrow} + u_{n\downarrow}v^*_{n\downarrow}. \tag{C9}$$

For the other equal-spin component f_2 [Eq. (10c)], it is straightforward to show that

$$\begin{aligned} u'_{n\uparrow}v'^*_{n\uparrow} - u'_{n\downarrow}v'^*_{n\downarrow} &= \cos\theta_i(u_{n\uparrow}v^*_{n\uparrow} - u_{n\downarrow}v^*_{n\downarrow}) \\ &\quad + i\sin\theta_i\left(u_{n\uparrow}v^*_{n\downarrow} - u_{n\downarrow}v^*_{n\uparrow}\right), \\ &= \cos\theta_i f_2 + i\sin\theta_i f_0. \end{aligned} \tag{C10}$$

* chientewu@nctu.edu.tw
† klaus.halterman@navy.mil

[1] J. Linder and J.W.A. Robinson, Nat. Phys. **11** 307 (2015).
[2] O. Sangjun, D. Youm and M.R. Beasley, App. Phys. Lett. **71**, 2376

(1997).
[3] L. R. Tagirov, Phys. Rev. Lett.**83**, 2058 (1999).
[4] A. I. Buzdin, A. V. Vedyayev, and N. V. Ryzhanova, Europhys. Lett. **48**, 686 (1999).
[5] S. Takahashi, S. Hikino, M. Mori, J. Martinek, and S. Maekawa, Phys. Rev. Lett.**99**, 057003 (2007).
[6] Zh. Devizorova and S. Mironov, Phys. Rev. B**95**, 144514 (2017).
[7] S. Mironov and A. Buzdin, Phys. Rev. B**92**, 184506 (2015).
[8] J. A. Ouassou, A. Pal, M. Blamire, M. Eschrig, and J. Linder, Scientific Reports **7**, 1932 (2017).
[9] A. Srivastava, L. A. B. Olde Olthof, A. Di Bernardo, S. Komori, M. Amado, C. Palomares-Garcia, M. Alidoust, K. Halterman, M. G. Blamire, and J.W.A. Robinson, Phys. Rev. Applied **8**, 044008 (2017).
[10] R.S. Keizer, S.T.B. Goennenwein, T.M. Klapwijk, G. Miao, G. Xiao and A. Gupta, Nature **439**, 825 (2006).
[11] M. S. Anwar, F. Czeschka, M. Hesselberth, M. Porcu, and J. Aarts, Phys. Rev. B**82**, 100501(R) (2010).
[12] F. S. Bergeret, A.F. Volkov, and K.B. Efetov, Phys. Rev. Lett.**86**, 4096 (2001).
[13] C.-T. Wu, Oriol T. Valls, and Klaus Halterman, Phys. Rev. B**86**, 014523 (2012).
[14] M. Eschrig, J. Kopu, J. C. Cuevas, and Gerd Schön, Phys. Rev. Lett.**90**, 137003 (2003).
[15] A. V. Galaktionov, M. S. Kalenkov, and A. D. Zaikin, Phys. Rev. B**77**, 094520 (2008).
[16] V. N. Krivoruchko and V. Yu. Tarenkov, Phys. Rev. B**75**, 214508 (2007).
[17] V. Peña, Z. Sefrioui, D. Arias, C. Leon, J. Santamaria, M. Varela, S. J. Pennycook, and J. L. Martinez, Phys. Rev. B**69**, 224502 (2004).
[18] Y. Kalcheim, O. Millo, M. Egilmez, J. W. A. Robinson, and M. G. Blamire, Phys. Rev. B**85**, 104504 (2012).
[19] C. Visani, Z. Sefrioui, J. Tornos, C. Leon, J. Briatico, M. Bibes, A. Barthélémy, J. Santamaría, and Javier E. Villegas, Nat. Phys., **8**, 539 (2012).
[20] D. Sprungmann, K. Westerholt, H. Zabel, M. Weides, and H. Kohlstedt, Phys. Rev. B**82**, 060505 (2010).
[21] A. Singh, S. Voltan, K. Lahabi, and J. Aarts, Phys. Rev. X **5**, 021019 (2015).
[22] J. Zhu, I.N. Krivorotov, K. Halterman, and O.T. Valls, Phys. Rev. Lett.**105**, 207002 (2010).
[23] A.A. Jara, C. Safranski, I.N. Krivorotov, C.-T. Wu, A.N. Malmi-Kakkada, O.T. Valls, and K. Halterman Phys. Rev. B**89**, 184502 (2014).
[24] M. G. Flokstra, T. C. Cunningham, J. Kim, N. Satchell, G. Burnell, P. J. Curran, S. J. Bending, C. J. Kinane, J. F. K. Cooper, S. Langridge, A. Isidori, N. Pugach, M. Eschrig, and S. L. Lee, Phys. Rev. B **91**, 060501 (2015).
[25] P. V. Leksin, N. N. Garifyanov, I. A. Garifullin, Ya. V. Fominov, J. Schumann, Y. Krupskaya, V. Kataev, O. G. Schmidt, and B. Büchner, Phys. Rev. Lett.**109**, 057005 (2012).
[26] X. L. Wang, A. Di Bernardo, N. Banerjee, A. Wells, F. S. Bergeret, M. G. Blamire, and J. W. A. Robinson, Phys. Rev. B**89**, 140508 (2014).
[27] K. Halterman and M. Alidoust, Phys. Rev. B 94, 064503 (2016).
[28] X. Montiel, D. Gusakova, M. Daumens, and A. Buzdin, Europhys. Lett. **86**, 67002 (2009).
[29] M. Eschrig, Rep. on Prog. Phys. **78** 104501 (2015).
[30] K. B. Efetov, I. A. Garifullin, A. F. Volkov, and K. Westerholt, *Magnetic Heterostructures. Advances and Perspectives in Spin Structures and Spin Transport. Series Springer Tracts in Modern Physics*, Vol. **227**. Zabel H., Bader S. D. (Eds.), (2007), p. 252.
[31] A.A. Golubov, M.Yu. Kupriyanov, E, ll'ichev, Rev. Mod. Phys.**76**, 411 (2004).
[32] A.I. Buzdin, Rev. Mod. Phys.**77**, 935 (2005).
[33] Y. Asano, Y. Tanaka, and A. A. Golubov, Phys. Rev. Lett.**98**, 107002 (2007).
[34] Y. Sawa, Y. Tanaka, and Y. Asano, J. Phys. Chem. Solids **69**, 3247 (2008).
[35] M. Eschrig and T. Löfwander, Nat. Phys. **4**, 138 (2008)
[36] Z. M. Zheng and D. Y. Xing, J. Phys. Condens. Matter. **21**, 385703 (2009).
[37] H. Enoksen, J. Linder, and A. Sudbø, Phys. Rev. B**85**, 014512 (2012).
[38] F. Giazotto, J.T. Peltonen, M. Meschke, and J.P. Pekola, Nat. Phys. **6**, 254 (2010).
[39] P. Spathis, S. Biswas, S. Roddaro, L. Sorba, F. Giazotto, and F. Beltram, Nanotechnology **22**, 105201 (2011).
[40] M. Alidoust, K. Halterman, and J. Linder, Phys. Rev. B **88**, 075435 (2013).
[41] J.C. Slonczewski, J. Magn. Magn. Mater. **159**, L1 (1996).
[42] L. Berger Phys. Rev. B **54**, 9353 (1996).
[43] J. Linder, A. Brataas, Z. Shomali, and M. Zareyan, Phys. Rev. Lett. **109** 237206 (2012).
[44] P.D. Sacramento and M.A.N. Araújo, Eur. Phys. J. B **76**, 251 (2010).
[45] K. Halterman and M. Alidoust, Supercond. Sci. Technol. **29**, 055007 (2016).
[46] A. Fert, Rev. Mod. Phys. **80** 1517 (2008).
[47] A. Brataas, A.D. Kent, and H. Ohno, Nat. Mat. **11**, 372 (2012).
[48] G.E.W. Bauer, E. Saitoh, and B.J. van Wees, Nat. Mat. **11**, 391 (2012).
[49] V. Braude and Yu. V. Nazarov, Phys. Rev. Lett.**98**, 077003 (2007).
[50] M. Eschrig, T. Löfwander, T. Champel, J. C. Cuevas, J. Kopu, and Gerd Schön, J. Low Temp. Phys. **147**, 457 (2007)
[51] R. Grein, M. Eschrig, G. Metalidis, and Gerd Schön, Phys. Rev. Lett.**102**, 227005 (2009).
[52] M. Eschrig, A. Cottet, W. Belzig, and J. Linder, New J. Phys. **17**, 083037 (2015).
[53] K. Halterman, O.T. Valls, and C.-T. Wu, Phys. Rev. B**92**, 174516 (2015).
[54] M. Bozovic and Z. Radovic, Phys. Rev. B**66**, 134524 (2002).
[55] Z. Radovic, N. Lazarides, and N. Flytzanis, Phys. Rev. B**68**, 014501 (2003).
[56] C.W.J. Beenakker, Phys. Rev. Lett. **97**, 067007 (2006).
[57] M.J.M. de Jong, C.W.J. Beenakker, Phys. Rev. Lett. **74**, 1657 (1995); C.W.J. Beenakker, Lect. Notes Phys. **667**, 131 (2005).
[58] J.W.A. Robinson, J.D.S. Witt, and M.G. Blamire, Science **329**, 59 (2010).
[59] T.S. Khaire, M.A. Khasawneh, W.P. Pratt, Jr., and N.O. Birge, Phys. Rev. Lett.**104**, 137002 (2010).
[60] Y. Asano, Y. Sawa, Y. Tanaka, and A. A. Golubov Phys. Rev. B**76**, 224525 (2007).
[61] C.-T. Wu, O.T. Valls, and K. Halterman, Phys. Rev. B**90**, 054523 (2014).
[62] E. Moen and O.T. Valls, Phys. Rev. B**95**, 054503 (2017).
[63] E. Moen and O.T. Valls, Phys. Rev. B**97**, 174506 (2018).
[64] C. D. Feng, Z. M. Zheng, R. Shen, B. Wang, and D. Y. Xing, Phys. Rev. B**81**, 224510 (2010).
[65] J. Linder, M. Cuoco, and A. Sudbø, Phys. Rev. B**81**, 174526 (2010).
[66] B. Béri, J. N. Kupferschmidt, C. W. J. Beenakker, and P. W. Brouwer, Phys. Rev. B**79**, 024517 (2009).
[67] J. N. Kupferschmidt and P. W. Brouwer, Phys. Rev. B**83**, 014512 (2011).
[68] F. B. Wilken and P. W. Brouwer, Phys. Rev. B**85**, 134531 (2012).
[69] J. Linder, T. Yokoyama, and A. Sudbø, Phys. Rev. B**79**, 224504

(2009).
[70] P.G. deGennes *Superconductivity of Metals and Alloys*
[71] C.-T. Wu, O.T. Valls and K. Halterman, Phys. Rev. B**86**, 184517 (2012).
[72] G. E. Blonder, M. Tinkham, and T. M. Klapwijk, Phys. Rev. B**25**, 4515 (1982).
[73] K. Halterman, P.H. Barsic, and O. T. Valls, Phys. Rev. Lett.**99**, 127002 (2007).
[74] K. Halterman, O.T. Valls, and P.H. Barsic Phys. Rev. B**77**, 174511 (2008).
[75] K.Halterman and M. Alidoust, Phys. Rev. B**94**, 064503 (2016).
[76] M. Alidoust, K. Halterman, and O.T. Valls, Phys. Rev. B **92**, 014508 (2015).
[77] X. Waintal and P.W. Brouwer, Phys. Rev. B**65**, 054407 (2002).